ALEPH 91-26
PHYSIC 91-25
S. Roehn, A. Stahl
20.2.1991

Measurement of τ Polarisation in $\tau \rightarrow \mu \nu_\tau \nu_\mu$ Decays

Steffen Roehn
Institut für Physik, Universität Mainz

Achim Stahl
Institut für Hochenergiephysik, Universität Heidelberg

February 8, 1991

Abstract

Based on the data taken in 1989 and 1990, 1401 $\tau \rightarrow \mu \nu_\tau \nu_\mu$ decays are selected to measure the momentum spectrum of the μ. From this distribution the τ polarisation has been determined. The corresponding polarisation is $P_\tau = (-19 \pm 12_{stat} \pm 5_{syst})\%$.

1 Introduction

The polarisation of the τ's produced at the Z_0 pole can be extracted from the momentum spectrum of the final decay particle. This note describes in great detail the analysis using the channel $\tau \rightarrow \mu \nu_\tau \nu_\mu$ to measure the mean polarisation of the τ. It shall help to get all information about the methods and numbers in the corresponding ALEPH publication.

2 Selection and Background

2.1 Preselection

The selection of the $\tau \rightarrow \mu \nu_\tau \nu_\mu$ decays starts from EDIR class 15. We need the definition of a good track, which has to fulfil

At least 4 TPC hits,
Momentum larger than 0.1 GeV/c,
$z_0 < 10cm$, and
$d_0 < 2cm$.

The applied cuts for CLASS 15 are:

- P.1 At least 2, but not more than 8 good tracks in the event.
- P.2 At least one track per hemisphere (the thrust axis defines the hemispheres).
- P.3 At least one track with a momentum larger than 3 GeV/c.
- P.4 No track with an opening angle to the corresponding jet axis, which fulfills $cos(\eta) < 0.85$, if more than 4 good tracks are found.

In the case of exactly 2 tracks, it is sufficient that both tracks have $d_0 < 5cm$.

The Preselection is applied for technical reasons, to save computing time. All the cuts will be reinforced in the further selection. Therefore it is not necessary to study them in detail.

2.2 Event Selection

It is very important for this analysis to ensure that HCal was working well for all the analysed events. For this reason several checks on the quality of the data have been made. These checks are explained in detail in subsection 2.10. From now on the resticted sample with properly working HCAL is used.

Going to the selection procedure, good tracks have to fulfil:

At least 4 TPC hits.
Momentum larger than 0.1 GeV/c
Momentum lower than 500. GeV/c
$z_0 < 10cm.$
$d_0 < 2cm.$

We then divide the event into two hemispheres, using the thrust axis. We require that there are

E.1 At least 2 good tracks in the event.
E.2 Not more than 6 good tracks in the event.
E.3 At least 1 good track per hemisphere.

To reduce the background coming from two-photon-exchange processes we further require that

E.4 The cosine of the angle between the two jets is below -0.9 (Acolinearity).
E.5 There is less than 20 GeV of total 'wire' energy in LCal.

We now look at the individual tracks. A track will be accepted as a μ coming from a τ-decay if it passes the following cuts:

S.1 No further good track in that hemisphere.
S.2 $x_\mu = \frac{p_\mu}{E_{Beam}} > 0.1.$
S.3 $|cos(\theta)| < 0.9$, where θ is the angle of the μ w.r.t the beam line.
S.4 μ–identification as described in the following chapter.

The cut S.2 must be applied to assure a full penetration of all the μs throughout whole ALEPH. Below $x_\mu = 0.1$ this is no longer true. The identification efficiency rapidly falls off and the spectrum gets strongly biased.

With cut S.3 we reject μs in the very forward region. There they only partially cross the TPC and the momentum resolution gets bad.

To reject muons from the process $Z^0 \rightarrow \mu^+\mu^-$, we apply a two cuts on the most energetic track on the recoiling side:

R.1 $x_{recoil} = \frac{p_{recoil}}{E_{Beam}} < 0.75.$
R.2 no μ–pre–identification (described in the following chapter) for the recoil side.

This restriction of the μ-pair-rejection to the recoiling side is very important. For τ decays, the momenta in the two hemispheres are independent. (There is a correlation between the two sides due to the spin correlation of the two τs, but this is very small.)

Therefore selection efficiency for μs from τ-decays is flat with momentum even around $x_\mu = 1.$, where the huge background is strongly suppressed.

The cuts R are only applied to the track with highest momentum on the recoiling side. This is to recover some efficiency for multiprong decays of the recoiling τ, which would get sometimes lost due to mis(pre)identification of one of the hadrons.

These cuts not only reject background from the process $Z^0 \to \mu^+\mu^-$, but also from the two-photon-exchange process $e^+e^- \to e^+e^-\mu^+\mu^-$ and from cosmic rays. Furthermore it rejects μs from τ decays too, if both τs decay into μs. This is 18% of the signal.

2.3 μ Identification

A μ is identified via its characteristic digital pattern in HCal. Additional information from ECal and the μ-chambers is only used for test purposes.

The first step in the μ-identification is the assignment of hits to the reconstructed tracks (see figure 1). The tracks are extrapolated from the outer TPC radius throughout the whole ALEPH detector. In HCal, plane by plane, the distance of each hit to the extrapolated track is calculated. If it is smaller than a certain value, it is assigned to the track. This procedure is called the road analysis and the maximum accepted distance between tracks and hits is called the width of the road. This width might vary from application to application. It typically consisits of a constant term and one varying with depth, taking into account the expected deviation of the real track from the extrapolation due to multiple scattering. This deviation grows typically up to a few centimeters at the last plane. The program not only looks for hits in the module hit by the extrapolation, but also searches the two adjacent modules. This becomes important for wide roads.

Within the road analysis the number of planes expected to be hit by a penetrating particle is calculated. The following dead zones are taken into account:

Barrel	Cracks between the modules and halfmodules.
Overlap	Dead zones between barrel and endcaps, including the notches at the end of the barrel modules.
Endcap	Cracks between the modules.
	Spacers between the tubes.
Whole detector	Tubes that weren't read out.

These are the most important dead zones. Others are missing like the spacers in the barrel, the chimney or chains with high voltage turned off.

To identify μs we define two variables, the first called **penetration**, the second **mean shower width**. The penetration looks at the ten outermost planes of HCal. There the number of planes having at least one associated hit are counted. To get the penetration we use a small road, having a half width of 2 cm plus 3σ of the expected deviation due to multiple scattering.

To calculate the mean shower width we redo the road analysis with a much wider

road, wide enough to contain the main part of a hadronic shower. We have chosen a halfwidth of 30 cm plus 3σ of the multiple scattering cone. Plane by plane we calculate the maximum distance between associated hits. The average over all the fired planes gives the mean shower width.

The cuts for μ-identification are :

M.1	Penetration	At least 4 fired planes (within last 10). road : $2cm + 3\sigma_{M.S.}$
M.2	Mean shower width	in *Barrel* less than 2.8 cm. in *Endcap* less than 4.0 cm. road : $30cm + 3\sigma_{M.S.}$

The mean shower width for μs is different in barrel and endcaps. Therefore we have chosen different values for the cut M.2 to achieve the same efficiency in barrel and endcaps. The reason for this difference is a geometrical one. If a particle crosses a plane in HCal not perpendicular to it, it might happen that more than one tube fires. (This is not the only reason for multiple hits produced by a single particle.) The mean shower width increases. Due to the different geometry of the endcap modules, larger deviations from perpendicular impact are possible there. See figure 2 for an illustration of these distributions.

For the μ–pre–identification, used to reject μ-pair background, we cut on penetration only to reach a higher efficiency:

PR.1	Penetration	$\frac{NUMBER\ OF\ FIRED\ PLANES}{NUMBER\ OF\ EXPECTED\ FIRED\ PLANES} \geq 0.2$ (within last 10 planes).

If the track is in active zones throughout all 10 planes this is equivalent to the requirement of at least two fired planes. If the track partially hits dead zones the requirement is looser which ensures a high efficiency.

2.4 Acceptance Calculation

The acceptance of all cuts except μ-identification was calculated using Monte Carlo. Table 1 shows their efficiencies.

More important than the absolute value of the efficiency is its dependence on the μ-momentum. Only this enters the polarisation measurement. This has also been studied using Monte Carlo. A slope in the efficiency is produced only by a few cuts. These are E.3, E.4 and R. E.3 and E.4 cut events with hard initial state radiation. The cuts R produce a small slope due to spin-spin-correlations between the two τs. The total slope is $(4.6 \pm 1.8)\%$ (see figure 3). This value includes smearing due to momentum resolution.

cut	efficiency (in %)
E.1	92.6 ± 0.3
E.2	99.98 ± 0.02
E.3	97.8 ± 0.1
E.4	99.3 ± 0.1
E.5	99.96 ± 0.02
E	91.8 ± 0.3
S.1	99.7 ± 0.1
S.2	85.5 ± 0.4
S.3	91.9 ± 0.3
S	78.0 ± 0.4
R.1	93.8 ± 0.3
R.2	77.6 ± 0.4
R	73.3 ± 0.5
all	52.7 ± 0.5

Table 1: Acceptance for different cuts

2.5 Efficiency of μ-Identification

To measure the efficiency of the μ-identification we select a testsample of μs. It is that this selection is independent of the μ-identification. Therefore we use only the μ–chambers, not the HCal. The cuts are (**testsample 1**):

E.1 to E.5	Eventselection, see chapter 2.2.
S.1 to S.3	Trackselection, see chapter 2.2.
MC.1	At least 1 associated hit in a μ-chamber.

The testsample contains μs of different momenta and different directions. We use it to study variations of the μ-identification efficiency with x_μ and $cos(\theta)$. It is clear that it is not usefull to study the breakdown of selection efficiency due to stopping μs at very low momenta. Those μs do not enter the testsample. Hits in the μ-chambers are associated to a track up to distances of about $25cm$ (We use the standard MCAD bank). We use that large value to ensure that we do not loose μs due to a bad extrapolation. This would bias the efficiency measurement. Figure 4 illustrates that 25cm is a safe value.

Figures 5 and 6 show the efficiencies of the μ-identification and μ–pre–identification measured with the testsample. The momentum dependence is well reproduced by a linear fit through the datapoints (excluding the bin below $x_\mu = 0.1$). The slopes we get are $(+2.4 \pm 1.2)\%$ and $(0.8 \pm 0.6)\%$. These small but non zero slopes are believed to be due to larger uncertainties in the extrapolation at lower momenta, where the bending plays a more important role. The efficiencies are flat in $cos(\theta)$ within the barrel and the

endcaps, but we see a clear drop of efficiency in the overlap.

The absolute values of the efficiencies measured with testsample 1 have to be treated with care for two reasons. In 1989 the μ-chambers had bad efficiencies. This part of data, in which the identification efficiency was smaller too, is underrepresented in the testsample. Secondly the cracks between the μ-chambers in the barrel match those of HCal, so that they are not properly included in the testsample. To get the absolute values of the efficiencies we use a second testsample. It contains events from the process $Z^0 \rightarrow \mu^+\mu^-$. It is based on tracks and ECal information only. **Testsample 2** is defined by the cuts:

E.1 to E.5	Eventselection, see chapter 2.2.
MP.1	Exactly 2 good tracks in the event.
MP.2	$0.8 < x < 1.2$ for both tracks.
MP.3	$\|cos(\theta)\| < 0.9$ for both tracks.
MP.4	$ECal_{wire} < 5GeV$

$ECal_{wire}$ is the ECal wire energy in the module hit by the track and the adjacent ones. Figure 7 shows the $ECal_{wire}$ of all pairs.

Table 2 shows the results (all values in %):

	EFFICIENCIES:			
	full testsample 2		cracks excluded	
	μ-id	μ-pre-id	μ-id	μ-pre-id
BARREL 89:	81.4 ± 1.3	92.9 ± 0.9	85.4 ± 1.3	96.9 ± 0.6
ENDCAP 89:	68.4 ± 2.2	93.0 ± 1.2	70.6 ± 2.2	94.3 ± 1.1
1989:	76.8 ± 1.1	92.9 ± 0.7	80.1 ± 1.1	95.9 ± 0.6
BARREL 90:	86.6 ± 0.4	95.2 ± 0.3	91.2 ± 0.4	99.0 ± 0.1
ENDCAP 90:	84.3 ± 0.5	96.6 ± 0.3	86.4 ± 0.5	98.0 ± 0.2
1990:	85.6 ± 0.3	95.8 ± 0.2	89.2 ± 0.3	98.6 ± 0.1
ALL:	84.7 ± 0.3	95.5 ± 0.2	88.3 ± 0.3	98.3 ± 0.1

Table 2: Efficiencies for μ–idenification and μ–pre–identification

To check this measurement we compare the numbers with those determined from testsample 1 at 45 GeV. To make them comparable, the 1989 data and the barrel cracks (requiring more than 5 expected fired planes within last 10) have to be excluded in both samples, because of the problems with the absolute value from testsample 1 as mentioned above. The comparison (see table 3) shows a maximal deviation of 3% for the μ–identification and 1.5% for the μ–pre–identification. These deviations are taken as errors on the measurements of the efficiencies which are then

$$\epsilon_{\mu-ID} = (84.7 \pm 3.0)\%$$

μ-id		
	testsample 1	testsample 2
BARREL	89.1 ± 1.4	91.2 ± 0.4
ENDCAP	87.2 ± 1.6	84.3 ± 0.5
μ-pre-id		
	testsample 1	testsample 2
BARREL	98.1 ± 0.7	99.0 ± 0.1
ENDCAP	98.0 ± 0.8	96.6 ± 0.3

Table 3: Comparison of efficiencies from testsample 1 and 2

$$\epsilon_{\mu-pre-ID} = (95.5 \pm 1.5)\%.$$

One might worry about noise in the μ-chambers creating fake μs in testsample 1. To check this we selected a third testsample of $Z^0 \rightarrow e^+e^-$ and counted the number of hits in the μ-chambers. The cuts of **testsample 3** are:

E.1 to E.5	Eventselection, see chapter 2.2.
EP.1	Exactly 2 good tracks in the event.
EP.2	$0.8 < x < 1.2$ for both tracks.
EP.3	$\|cos(\theta)\| < 0.9$ for both tracks.
EP.4	$ECal_{wire} > 80GeV$

This study was done some time ago when the full statistic was not yet available. From 2750 tracks that passed the cuts none had an associated hit in a μ-chamber. For HCal we found a probability of $(9 \pm 2) \cdot 10^{-4}$ to get a hit in one of the last 10 planes in the small road of cut M.1.

2.6 Background from $\tau \rightarrow hadrons$

This is the most serious background, giving the largest systematic error. Therefore special care has to be taken. Especially we want to avoid using the detector simulation of hadrons for the estimation of the misidentification. But we have to use Monte Carlo to get the kinematics. We start from Monte Carlo. We select all hadronic τ-decays by Monte Carlo truth and apply all kinematical cuts (E; R; S.1,S.2,S.3). Figure 8 shows the Monte Carlo truth of the tracks that survived the cuts. There are 2.5 times more hadrons than μs. This is the problem π/μ-separation has to fight with. (Beside the πs there are also Ks in τ-decays. It is assumed that their behaviour is simular to that of the πs and they are treated together.)

The study of the hadron rejection due to μ-identification (cut S.4) is done with **testsample 4** from data. It consists of events from decays $\tau \rightarrow hadron + \geq 1\pi^0$. These events are tagged by identifying the π^0(s) in ECal. No cut is applied on the

charged track, so that we get an unbiased sample of hadrons. Again it is essential that the μ-identification only uses HCal. We do not risk to bias the testsample with the ECal cuts. The cuts are:

	E.1 to E.5	Eventselection, see chapter 2.2.
	S.1 to S.3	Trackselection, see chapter 2.2.
	R.1 and R.2	μ-pair rejection, see chapter 2.2.
	PI.1a	At least 3 photons nearby the track.
or	PI.1b	Two neutral ECal clusters nearby the track, having an invariant mass of $(140 \pm 60) MeV$.
or	PI.1c	A neutral ECal cluster nearby the track, having a Bulos mass of $(110 \pm 50) MeV$.
	PI.2	$ECal_{wire}/E_{beam} < 0.75$ in the recoiling hemisphere.

(A track enters the testsample if it fulfills at least one of the conditions PI.1.)
Neutral ECal clusters are defined by the following cuts:

NC.1	No link to a charged track (bank PCRL).
NC.2	At least 100 MeV in stack 1.
NC.3	At least 100 MeV in stack 2.

In cut PI.1a photons are defined as local maxima in ECal clusters by a program written by Zhang. The Bulos mass used in PI.1c is an approximation of the invariant mass of two photons merged in one cluster. It is derived from the energy of the cluster and its shape of the cluster, giving a measurement of the angle between the two photons. It is assumed that the energy is shared symmetrically between the two photons. This is why the Bulos mass is systematically smaller as the invariant mass. Program and description, can be found on the UPHY disk. Cut PI.1a mainly tags πs from the decay $\tau \rightarrow a_1 \nu_\tau \rightarrow \pi^\pm \pi^0 \pi^0 \nu_\tau$, whereas cuts PI.1b and PI.1c tag events of the type $\tau \rightarrow \rho \nu_\tau \rightarrow \pi^\pm \pi^0 \nu_\tau$.

Figure 9 shows the distributions of the variables of cut PI.1 in comparison with Monte Carlo, which is used to ensure that this testsample is free from μ-background. This study was done with older routines for counting local maxima written by Orteo and doesn't include cut PI.2. It has not yet been updated with Zhangs version. Figure 10 gives the Monte Carlo truth information of tracks that have been tagged from a sample of 10k τ-Monte Carlo and the corresponding number of $e^+e^- \rightarrow e^+e^-$ and $e^+e^- \rightarrow \mu^+\mu^-$. We do not find any μ-background and 5.4 electrons ($1\ \tau \rightarrow e\nu_e\nu_\tau$ and 4.4 $e^+e^- \rightarrow e^+e^-$).

Finally we find 1278 tagged π^0 in the whole data sample. Their spectrum is shown in figure 11 in comparison with the spectrum of the hadrons we hav e to fight against (from Monte Carlo). The testsample contains less events at higher energies.

Now we can use this testsample and the ones defined in chapter 2.5 to study the π/μ-separation. This is shown in the figures 12. If we apply the μ-identification to testsample 4, 13 events survive. These give an average π-misidentification of

$$\epsilon_\pi = (1.0 \pm 0.3)\%. \quad (1)$$

Those misidentified events are dominated by decays in flight of the π and sail through.

Although statistics is quite poor, we tried to determine the momentum dependence of ϵ_π too. We calculated ϵ_π for 10 momentum bins and fitted a straight line through it, fixing the average to the value above. The slope we find is $(-0.2 \pm 1.6)\%$. (Monte Carlo gives $(-0.9 \pm 0.6)\%$.) See figure 13.

Now we are able to calculate the background spectrum. We start from the Monte Carlo spectrum of $\tau \rightarrow$ *hadrons*, apply the kinematical cuts (E, S.1 to S.3, R) (see figure 11) and multiply it with the above π-misidentification. The correction spectrum is shown in figure 14. The total background from those sources amounts to 52 ± 17 events.

Figure 22 shows another crosscheck of the background from $\tau \rightarrow$ *hadrons*. The Ecal wire energy in the moduls hit by the final μ–sample is plotted. There are 58 events with an energy larger than 2 GeV, which is untypical for μs. The large electromagnetic energy in those events might come from radiative $\tau \rightarrow \mu\nu_\mu\nu_\tau$ decays or from π^0s in $\tau \rightarrow$ *hadrons* decays. From Monte Carlo we expect 35 ± 6 radiative $\tau \rightarrow \mu\nu_\mu\nu_\tau$ decays and from the background estimation (section 2.6) we expect 52 ± 17 events from $\tau \rightarrow$ *hadrons*, about 80% of them accompanied by π^0s. This agrees well within errors with the 58 events we find.

2.7 μ–Pair Background

In this section we describe the correction of the spectrum for events with 2 μ in the final state. Those events should be rejected by cut R.2. But if one of the two μ fails the pre–identification it might enter the final sample. The correction includes background events from the processes $Z^0 \rightarrow \mu^+\mu^-$ and $e^+e^- \rightarrow e^+e^-\mu^+\mu^-$ and from cosmic rays as well as τ-events where both τs decayed into a μ.

The subtraction starts with the following equation,

$$1 = (\epsilon_\mu)^2 + 2(1 - \epsilon_\mu)\epsilon_\mu + (1 - \epsilon_\mu)^2 \quad (2)$$

giving the probability to identify both (1st term), only one (2nd term) or none (last term) of the μs out of a pair. Where ϵ_μ is the probability to identify a single μ (see section 2.5). We can count the number of events where we identified 2 μ and we have measured ϵ_μ so we can calculate the number of events, where we missed one of the μs. This is the number of events we have to subtract (43.6 in total).

To get their spectrum we take the events with 2 identified μ and assume that we missed one. We than apply all the cuts on those events (E, S, R.1). The remaining ones, normalized to the above number, give the correction spectrum. It is shown in figure 15.

2.8 Background from 2-Photon-Exchange Processes

Two-photon-exchange processes with μs in the final state may produce background. (If we believe Monte Carlo, the contribution from $e^+e^- \rightarrow e^+e^-e^+e^-$ and $e^+e^- \rightarrow e^+e^-q\bar{q}$

is negligible and $e^+e^- \rightarrow e^+e^-\mu^+\mu^-$ and $e^+e^- \rightarrow e^+e^-\tau^+\tau^-$ contribute about equally. The μ final state is suppressed with respect to the τs because of cut R.2, but has a larger cross section.) First we want to point out that we do not correct for this background. We only estimate its size and derive an upper limit of the systematic error from it. This estimation is done via an extrapolation in $cos(acol)$, the cosine of the angle between the two jets. For τ-pairs this is expected to be peaked near -1, whereas the background is approximately flat. Figure 16 shows this distribution for the real data in comparison with τ - Monte Carlo in the upper two histograms and for 2-photon - Monte Carlo in the lower two histograms. (All cuts applied except E.4.)

First we look at the τ - Monte Carlo. We find 11 events outside the region of the cut, corresponding to 9 events, if normalized to the luminosity of the data sample. But from data we find 30 events in that region. This is an excess of 21 events, indicating 2-photon background. From the two lower plots (2-photon Monte Carlo) in figure 16 we see that 1 event in the signal region corresponds to about 3 events outside. Taking this ratio from Monte Carlo we estimate 7 (21 times 1/3) background events in the final sample.

The part of this background, which is coming from the μ final state is in principle included in the μ-pair correction (section 2.7). But the size is underestimated, because an efficiency of 95.5% independent of momentum is assumed, which is not valid at the typically very low momenta of 2-photon events. For this reason and also because the τ - final state contributes, we conclude that the background subtraction is too small. But the remaining background cannot be larger than 7 events, as we have estimated above. This is the final number we will use to get the systematic error.

2.9 Other Small Background

2.9.1 Hadronic Background

In July 1990 (about half of the statistics taken) we scanned all events having between 4 and 7 good tracks in the recoiling hemisphere. We found 6 events, which looked like τs (2 events $\tau \rightarrow 3\pi + V_0$; 2 events $\tau \rightarrow 3\pi + conv.\gamma$, 1 event $\tau \rightarrow 3\pi$ having one track reconstructed as two and 1 τ with interaction in μ-vertex) and one $q\bar{q}$, which is finally killed by E.2. From that we conclude that the hadronic background is negligible.

2.9.2 Cosmic Background

Figure 17 shows the total number of hits in ITC in all the accepted events. There are 5 events with no hits giving an upper limit on the cosmic background. This background is included in the μ-pair correction and the remaining uncertainty is negligible.

2.9.3 Background from e^+e^--pairs and $\tau \rightarrow e\nu_e\nu_\tau$

In chapter 2.5 we have estimated the probability for electrons to produce a hit in the last 10 planes of HCal. From that we conclude that this background is negligible.

2.10 Data Quality Requirements

This analysis depends on the performance of the HCAL. Especially the μ-pair rejection is sensitive to hardware failures. To set up our list of "good" runs and events we started from all the runs declared as "MAYBE" or "PERFECT" by run quality and made the following checks:

(i) Event by event we checked the presence of HCal readout. We looked for the header of the HTUB bank. (We require that EVEH, XTEB, PFRF, PEST and PEWI were present too.)

(ii) We required XLUMOK to be true (Main high voltage bits set and main triggers enabled.)

(iii) For 1989 data, we checked all entries concerning HCal in the online logbook .

(iv) For 1990 data, we checked all warnings concerning HCal from run quality.

(v) We divided the whole data in 44 subperiodes of data taking, following the time table of data taking and shutdowns. We created individual testsamples with the μ-chambers (see description of testsample 1 in section 2.5) for each of these subperiodes, separately for barrel and each of the endcaps. (Each testsample contains between 100 and 400 events.) We selected those μ, that failed the μ–pre–identification and plotted their ϕ-angles and $cos(\theta)$. We looked for accumulations of lost μs in individual modules. If we found such an accumulation we declared all events with μ-candidates pointing to that module or the one opposite to it as bad. Figure 18 shows an example of a bad module, that was killed by that procedure.

(vi) The same procedure was repeated with μs from testsample 2.

(vii) For short runs with empty testsamples we scanned $q\bar{q}$-events and looked for the presence of the digital readout.

(viii) We checked the masks of the digital chains and discarded endcap modules in a few runs, where only 5 planes were read out.

2.11 Momentum Calibration

Miscalibration of the tracking chambers might be another source of systematic errors. Our estimate of the influence of a calibration error on the polarisation measurement is based on studies done by Werner Wiedenmann ([1]). He has measured the deviation of μ-momentum from the beam momentum in $Z^0 \rightarrow \mu^+\mu^-$. He gets values between + and - 0.2% dependent on the charge of the μ and $cos(\theta)$. They are shown in Figure 19.

To correct our spectrum for these deviations we have to extrapolate the miscalibration measured at 45 GeV/c down to lower momentum. We assume it is produced by an offset in the sagitta, which leads to the following correction:

$$\frac{1}{p_t^{corr.}} = \frac{1}{p_t} + c_1 \tag{3}$$

The constant c_1 is determined from Werner's numbers at 45 GeV/c. It depends on $cos(\theta)$. We get about the same values for both charges. They are shown in figure 20. We have parametrized c_1 by a parabola. The fit gives

$$\begin{aligned} c_1(q=+1) &= (6.8\times10^{-4}cos^2(\theta) - 2.1\times10^{-4}cos(\theta) - 2.4\times10^{-4})c/GeV \\ c_1(q=-1) &= (8.9\times10^{-4}cos^2(\theta) - 1.5\times10^{-4}cos(\theta) - 2.3\times10^{-4})c/GeV. \end{aligned}$$

We have corrected the final spectrum with this procedure. The effect of the correction is shown in figure 21.

For testpurposes we used another correction:

$$\frac{1}{p_t^{corr.}} = c_2 \cdot \frac{1}{p_t}. \tag{4}$$

2.12 Final Spectrum

In total we identified 1401 $\tau \rightarrow \mu\nu_\mu\nu_\tau$ events. Their spectrum is shown in figure 21. This spectrum is not corrected neither for background nor for the slope in ϵ_μ.

3 Fitting Methods

The information about the τ polarisation is extracted from the momentum spectrum of the final μs. Their angle w.r.t. the beam line is not regarded in this anaylsis. This possibility of extracting the maximum information about various parameters (not only the polarisation) together with experimental results will be the topic of a future ALEPH-note ([3]). In this note detailed information of the underlying theoretical assumptions and equations will be given as well.

3.1 Basic formulas on the Born–level

The momentum distribution of the μ on the tree level is given by [4]

$$\frac{d\sigma^{Born}}{dx}(s,x) = F_0(s)h_0^\mu(x) + F_2(s)h_1^\mu(x), \tag{5}$$

where s is the center–of–mass energy squared ($s = 4E_{Beam}^2$) and $x = E_\mu/E_{Beam}$. The F_i and h_i^μ can be found in [4] and are given by:

$$F_0(s) = \frac{\pi\alpha^2}{2s}\left[2\Re\{\chi(s)\}q_e q_\tau v_e v_\tau + |\chi(s)|^2(v_e^2+a_e^2)(v_\tau^2+a_\tau^2) + q_e^2 q_\tau^2\right],$$

$$F_2(s) = \frac{\pi\alpha^2}{2s}\left[2\Re\{\chi(s)\}q_e q_\tau v_e a_\tau + |\chi(s)|^2(v_e^2+a_e^2)2v_\tau a_\tau\right],$$

$$h_0^\mu(x) = \frac{5}{3} - 3x^2 + \frac{4}{3}x^3,$$

$$h_1^\mu(x) = -\frac{1}{3} + 3x^2 - \frac{8}{3}x^3, \tag{6}$$

$$v_f = \frac{I_3^f - 2Q_f sin^2\theta_W}{2sin\theta_W cos\theta_W},$$

$$a_f = \frac{I_3^f}{2sin\theta_W cos\theta_W},$$

$$and\ \frac{v_f}{a_f} = 1 - 2\frac{Q_f}{I_3^f}sin^2\theta_W. \tag{7}$$

The standard "V-A" structure of the charged current has been assumed for the decay of the τ. This assumption will be dropped in [3].

On the peak ($s = M_Z^2$), equation (5) can be simplified to

$$\frac{d\sigma^{Born}}{dx}(s,x) \propto h_0^\mu(x) + A_\tau h_1^\mu(x), \tag{8}$$

$$A_\tau = \frac{2a_\tau v_\tau}{a_\tau^2 + v_\tau^2}. \tag{9}$$

Equation (5) is sensitive to the ratio A_τ only, not to the couplings v_τ and a_τ themselves. The mean τ polarisation is given by $P_{\tau^-} = -A_\tau$.

One is now able to use the momentum information of a track to extract the polarisation from equation (5). This is done by a fit of this equation to the momentum spectrum of the μs. The energy range has to be reduced to [0.1;0.95], because equation (5) is not valid at the edges of the spectrum (see [2]). Nevertheless, this accounts only to a very small loss in sensitivity. Furthermore the experimental circumstances require a minimal energy cut anyway.

3.2 Radiative Corrections

So far any radiative effect has been neglected. They are briefly discussed now. More detailed information can be found in [5,4,3,2].

Two different corrections have to be regarded (see [5]):

(i) "QED corrections". They consist of all one–loop diagrams with an extra real photon or a virtual photon–loop. As they form a gauge invariant subset and since they depend on the experimental cuts, it is sensible to separate them from the

(ii) "weak corrections". They consist of all the other possible one–loop diagrams as modifications of the propagator for γ, Z^0 and box diagrams with two massive boson exchanges.

While the "QED corrections" depend on the experimental conditions, the main bulk of the "weak corrections" can be taken into account by introducing "stared" and flavour dependent coupling constants. The tree level expressions can be used with these new coupling constants which are now a function of s (see [5,6,7]). The other weak effects are negligible compared to the experimental accuracy (see e.g. [2]).

The "QED corrections" are divided into

(i) *Kinematic Effects*, which account for a shift in x due to initial– and final–state radiation and bremsstrahlung of the decay product.

(ii) *Direct QED Effects*, which are essentially a spin flip of the τ. These effects change A_τ by -0.23% [4].

(iii) *Effects due to the Neglect of γ–Exchange*, which account for a shift of -0.09% in A_τ [4].

While the last two effects can be safely neglected, the kinematic effects result in a large correction (roughly $5-10\%$) of the polarisation. They are taken into account by a fragmentation model given in [4]. Equation (5) can then be rewritten as

$$\frac{d\sigma}{dx}(s,x) \propto W_0(s,x) + W_2(s,x),$$

$$\text{where } W_{(0/2)}(s,x) = \int_0^{1-x^2} \frac{dv}{\sqrt{1-v}} \rho(v) F_{(0/2)}(s(1-v)) H^\mu_{(0/1)}\left(\frac{x}{\sqrt{1-v}}\right). \quad (10)$$

The functions H^μ_0 and H^μ_1 are the general (radiative) case for the functions h^μ_i given in equation (6) and are given in [4], where $\rho(v)$ can be found as well.

3.3 Fit Procedure and Checks

The convolution in equation (10) is performed numerically taking into account the particular behaviour of the function $\rho(v)$. For each event the momentum $x = E_\mu/E_{Beam}$ of the μ and the squared CMS energy s is used to calculate a log–likelihood value according to equation (10). Using the different CMS energies guaranties the correct treatment of radiative corrections and s–dependent terms. The log–likelihood function is then maximized by MINUIT.

To see, which parameters have to be varied for this fit, equation (10) has to be compared with (5). It is clear that all manipulations due to QED radiative corrections mentioned above *do not change the structure* of the nonradiative equation. On the other hand, equation (10) depends nontrivially on the coupling constants a_i and v_i to the initial (e^+e^-) and the final state $(\tau^+\tau^-)$. This is due to the convolution of the F_i over the whole range of s, where they show a more complex dependence on a_i and v_i than "on peak". But, as the main contribution to the convolution comes from $s = M_Z^2$, this dependence is expected to be small.

Therefore some reference values for a_τ, a_e and v_e are used to perform a one–parameter (v_τ) log–likelihood fit. Those are taken as $a_\tau = a_e = -0.593$ and $v_e = -0.047$, which correspond to a $sin^2\theta_W$ of 0.230 used in the Monte Carlo simulation. They have not been changed since then because they are very close to the recent measurements of [8]: $a_{lepton} = -0.598 \pm 0.0041$ and $v_{lepton} = -0.040^{+0.040}_{-0.017}$. The fit to the momentum spectrum gives then a value for v_τ, which is used to get the polarisation via the relation $P_{\tau^-} = -\frac{2a_\tau v_\tau}{a_\tau^2+v_\tau^2}$. In [2] the dependence of this polarisation on variations of a_e, v_e and a_τ within more than twice of their errors have been studied. The resulting change in the polarisation is less than 0.23%. This shows that equation (10) is essentially a function of the ratio A_τ and not the couplings a_τ and v_τ themselves and justifies the procedure explained above.

To check the performance of the method described above a sample of 10000 $\tau \to \mu\nu\nu$ (KORALZ—generator level, momentum not smeared, all radiative effects switched on) is used. As the fitting method using equation (10) does—at this stage—not include the resolution effects, nonsmearing is appropriate to check the method. The input values for a_e and a_τ are -0.597, those for v_e and v_τ are -0.047 $(v/a = 0.079)$. This corresponds to a value of -15.6% for the polarisation. The range for $x = E_\mu/E_\tau$ is [0.1;0.95]. The result for the fit to this spectrum is $P_{\tau^-} = (-18.7 \pm 5.3)\%$, in good agreement with the expectation.

3.4 Treatment of Efficiency, Resolution and Background

To guarantee that the formalism given in the last section works properly on data, the efficiency, the momentum resolution and the background has to be taken into account. This is done by multiplying equation (10) with a global "Efficiency–function" $\epsilon(x)$, which is defined as

$$\epsilon(x) = \epsilon_{Acceptance}(x) \times \epsilon_{\mu-ID}(x) \times (1 + \epsilon_\pi(x) + \epsilon_{\mu\mu}(x)). \tag{11}$$

The various ϵ are explained below:

(i) $\epsilon_{Acceptance}$ includes the momentum resolution and the geometrical accepantce w.r.t. all cuts besides the μ–identification. While the absolute value does not enter in the final result, the slope is quite important. It is extracted from the full detector Monte Carlo. $\epsilon_{Acceptance}$ can be found in figure 3.

(ii) $\epsilon_{\mu-ID}$ is the measured efficiency for the μ–identification (see section 2.3) and is shown in figure 5. Again, the absolute value is not relevant.

(iii) ϵ_π is the amount of hadronic background (see section 4.4.1 and figure 14) related to the signal in the corresponding x bin.

(iv) $\epsilon_{\mu\mu}$ is the relative background from $\mu\mu$ events (see section 4.4.2 and figure 15).

4 Systematic Effects

4.1 Momentum Dependence of Selection Efficiency

In section 2.4 and 2.5 it was shown that there is a small momentum dependence of the acceptance and the μ-identification. To get the polarisation the spectum has been corrected for this variation with momentum. It is not nescessary to correct for the absolute size of the efficiency, because polarisation is determined only from the slope of the spectrum.

The slope of the acceptance was determined from Monte Carlo. It is $(4.6 \pm 1.8)\%$ (see section 2.4). This correction relies on the simulation of the kinematics of τ-events and the reconstruction of tracks. It is believed that this is accurate enough to produce only a negligible error on the slope measurement, compared to the statistical one. In addition the value of the polarisation in the Monte Carlo has in princible an influence on the slope of cut R.1 due to spin-spin-correlations. But this is also negligible compared to 1.8% statistical error on the slope. To estimate the systematic error, the slope was varied within the statistical error. The resulting systematic error from the acceptance correction is 1.8%.

The slope of the μ-identification was determined from testsample 1 (see section 2.5). It is $(2.4 \pm 1.1)\%$. It was varied by 1 σ, resulting in a change of polarisation by 1.2%.

4.2 Momentum Resolution

A correction of the smearing due to the finite momentum resolution is included in the above correction of acceptance. Its total contribution to the correction is only 1.6%. Therefore the error on it is negligible.

4.3 Momentum Calibration

The rescaling of the momentum described in section 2.11 changes the polarisation by 4.5% (Figure 21 shows both uncorrected and rescaled spectra.) To estimate the systematic error the correction constant c_1 was varied within the errors of the parabolic fit. In addition the rescaling scheme with c_2, using a factor instead of an offset in curvature, was tried. All changes of polarisation are within 0.5%.

4.4 Background

4.4.1 Background from $\tau \rightarrow$ *hadrons*

The total correction is 52 events compared to 1401 identified $\tau \rightarrow \mu\nu_\mu\nu_\tau$ in the raw spectrum. The main uncertainty comes from the lack of statistics in testsample 4 at higher momenta. Other uncertainties like branching ratios, background in testsample 4 or uncertainity of the simulation of the kinematics are negligible compared to that. To estimate the systematic error coming from this background correction we varied both the size of the misidentification $\epsilon_\pi = (1.0 \pm 0.3)\%$) and its slope $(-0.2 \pm 1.6)\%$ within the statistical errors. Figure 14 shows the correction spectrum together with the variations. The maximum change in polarisation we get is 3.8%.

4.4.2 Background from μ-Pairs

The final spectrum is further corrected for events with μ-pairs in the final state, that passed R.2. The determination of the correction spectrum is described in section 2.7 (see figure 15). It contains 43.6 events, but the bulk of this correction is not background. It is coming from τ events, both τs decaying into μ. From the shape of the correction spectrum, one might estimate the amount of background. It is approximately 12 events from $Z^0 \rightarrow \mu^+\mu^-$ and 4 two-photon-exchange events. The main uncertainty of this correction is coming from the measurement of the μ–pre-identification probability. It was determined to be $(95.5 \pm 1.5)\%$ in section 2.5. The error includes systematic effects. Variation of the correction within this error changes the polarisation by 0.2% at maximum.

4.4.3 Background from Two-Photon-Exchange Events

In section 2.8 an upper limit of 7 events on the size of this background was derived. Part of it is corrected with the above μ-pair correction, but we do not know how large this part is. About the spectrum of those events, we only know that they are low energetic. To get an upper limit on the systematic error, the worst case was assumed. 7 events were subtracted from the lowest bin, giving the largest allowed distortion of the slope of the spectrum. This changes polarisation by 1.6%.

5 Final Results

For the final result 1365 from 1401 μs are in the x range from 0.1 to 0.95. Performing a fit to those events as explained in section 3 leads to the results given in tables 4 and 5. These tables show the results of the systematic checks as well.

The final result for the polarisation is

$$P_{\tau^-} = \{-19.2 \pm 11.8_{stat.} \pm 5.2_{syst.}\}\ \%. \tag{12}$$

Method	*Difference to reference value in %*	*Resulting systematic error in %*
Final Result: shape of π misidentification from linear fit in x (Method A)	$P_{\tau^-} = -19.2^{+11.3}_{-12.2}$ %	
Background from $\tau \rightarrow$ hadron(s) (subsection 4.4.1)		± 3.8
shape of π misident. from MC (Method B)	-6.2	
shape of π misident. bin by bin as measured (Method C)	-5.4	
Method A: misident. probability + 1σ	-0.5	
Method A: misident. probability - 1σ	$+0.5$	
Method A: slope of misident. probability + 1σ	-3.6	
Method A: slope of misident. probability - 1σ	$+3.8$	
μ-pre-identification efficiency (subsection 4.4.2)		< 0.5
Efficiency changed by $+1\sigma$	-0.1	
Efficiency changed by -1σ	≈ 0	
Efficiency changed by $+3\sigma$	-0.2	
Efficiency changed by -3σ	$+0.1$	
μ-identification efficiency (subsection 2.3)		± 1.2
Slope of efficiency $+1\sigma$	$+1.1$	
Slope of efficiency -1σ	-1.2	
Slope of efficiency $+3\sigma$	$+3.5$	
Slope of efficiency -3σ	-3.5	

Table 4: *Results of systematic studies (π and μ background and μ efficiency).*

Method	*Difference to reference value in %*	*Resulting systematic error in %*
Momentum corrections (subsection 4.3)		±0.5
Momentum correction $+1\sigma$	+0.5	
Momentum correction -1σ	−0.3	
Momentum correction linear in x	−0.3	
No momentum correction at all	+4.5	
Background from 2 photon processes (subsection 4.4.3)		±2.8
Acollinearity < -0.9, no cut on LCAL energy	+2.9	
Data from Peak, $\pm 1GeV$ and $\pm 2GeV$, no cut on LCAL energy	+4.2	
Data from Peak and $\pm 1GeV$, no cut on LCAL energy	−3.1	
x_{recoil} or $E_{recoil} > 0.1$, no cut on LCAL energy	−2.1	
x_{recoil} or $E_{recoil} > 0.15$, no cut on LCAL energy	−3.1	
Acol. < -0.9, Peak, $\pm 1GeV$ and $\pm 2GeV$, LCAL energy < $20GeV$	+3.0	
first bin minus 7 events	−2.8	
Variation of the slope of the acceptance and resolution within 1σ (subsection 2.4)		±1.8
Total systematic error (added in quadrature)		±5.2

Table 5: *Results of systematic studies (Momentum correction and 2γ background).*

6 Acknowledements

We want to thank Steve Snows and Fabian Zomer, who have developped the idea of the mean shower width to identify $\tau \rightarrow \pi^{\pm}\nu_{\tau}$. Fabian has also done the modifications of the JULIA road analysis.

Thanks to Zhang, who wrote the routine to search for local maxima in ECAL clusters.

Furthermore we thank Nigel Keemer, who wrote the program for the calculation of the Bulos mass.

References

[1] W. Wiedenmann, ALEPH-note 90-156 (TPCGEN 90-8)

[2] St. Roehn, Ph.D. thesis (Mainz), in preparation.

[3] St. Roehn, A. Stahl, ALEPH-note, in preparation.

[4] G. Altarelli et al. (editors), Z Physics at LEP, **CERN 89-08 Volume 1** (1989) 235-265; (The sign for p given in equation 2.1 is wrong);
(Use *Erratum* from 8 March 1990).

[5] G. Altarelli et al. (editors), Z Physics at LEP, **CERN 89-08 Volume 1** (1989) 7-54.

[6] G. Altarelli et al. (editors), Z Physics at LEP, **CERN 89-08 Volume 1** (1989) 203-234.

[7] D.C. Kennedy, B.W. Lynn, **SLAC-PUB 4039** (1986, revised 1988).

[8] D. Decamp et al. (ALEPH Collaboration), *Z. Phys. C — Particles and Fields* **48** (1990) 365.

7 Figures

Figure 1: Example for the road analysis in HCAL. Described in detail in section 2.3.

Figure 2: Mean Shower Width of μ showing the difference between barrel and endcaps. From testsample 1, section 2.5.

Figure 3: Acceptance and Resolution from MC as function of x. For more details see section 2.4.

Figure 4: Number of hits in μ-chambers and their distance to the extrapolated track for testsample 1 and 2, section 2.5.

Figure 5: Efficiency of μ-identification as a function of x_μ and $cos(\theta)$. From testsample 1, section 2.5.

Figure 6: Efficiency of μ-pre–identification as a function of x_μ and $cos(\theta)$. From testsample 1, section 2.5.

Figure 7: $ECal_{wire}$ energy. Applied cuts E, MP.1, MP.3, $x_1 > 0.8, x_2 > 0.9$. Plot doesn't show the full statistic.

Figure 8: Monte Carlo truth of all τ-decays after kinematical cuts. The lower plot shows the decay channel, whereas the upper plot shows the identity of the charged particle seen in the detector. For example a decay $\tau \rightarrow \rho\nu_\tau$ will enter bin 8 of the lower plot, but bin 3 of the upper plot (if the π doesn't decay before reaching the calorimeters).

Figure 9: π^0-tagging (testsample 4): Comparison between data and Monte Carlo. Plot doesn't show the full statistic.

Figure 10: Monte Carlo truth of π^0 tagged events (testsample 4). See description of figure 8.

Figure 11: Spectra of hadrons from $\tau \rightarrow$ *hadrons* (Monte Carlo after kinematical cuts) and from testsample 4. Monte Carlo normalized to data.

Figure 12: π/μ-separation: Comparison between μ-signal and hadron-signal in HCal. See figure 2 as well. Plot doesn't show the full statistic.

Figure 13: π misidentification as a function of momentum. Fitted from testsample 4.

Figure 14: Correction spectrum of hadron background. The plot shows also the variations, that are used to determine the systematic error.

Figure 15: Correction spectra for μ-pairs. Still to be normalized to 43.6 events. On the histogram it is indicated, where one expects entries from the different processes.

Figure 16: Estimation of background from 2-photon-exchange processes. Applied cuts E.1, E.2, E.3, E.4, S and R. For details see section 2.8.

Figure 17: Total number of hits in ITC for all accepted events (upper plot) and for e^+e^--pairs (lower plot) from testsample 3.

Figure 18: Checks of HCal performance. ϕ-distribution of μs not preidentified in the barrel in the period of runs from 7530 to 7580. The plot clearly shows a lower efficiency in module 4 (from testsample 1). Therefore modules 4 and 10 weren't used for physics. The lower plot shows the penetration variable for halfmodule 11 in the barrel for the period of runs from 8869 to 9113. High voltage of planes 16 to 19 was turned off. The plot shows, that the preidentification efficiency is nevertheless above 90%. The module is not killed.

Figure 19: Momentum Calibration [1]. The two plots show the ratio p_μ/p_{beam} from events of the type $Z^0 \to \mu^+\mu^-$. The values are corrected for radiation.

Figure 20: Momentum Calibration. Correction of the calibration error by an offset in the sagitta. The plot shows the dependence of the correction constant c_1 and its parametrisation by a parabola. c_2 corresponds to another parametrisation.

Figure 21: Spectrum of the 1401 selected $\tau \to \mu\nu_\mu\nu_\tau$ decays. The spectrum is not corrected for background and efficiency.

Figure 22: Energy deposition in ECal of the 1401 selected $\tau \to \mu\nu_\mu\nu_\tau$ decays. (Twice the same plot with different scales.)

Figure 23: Final fit to the energy spectrum of the [m]s. The fit is explained in section 3.

Fig. 1

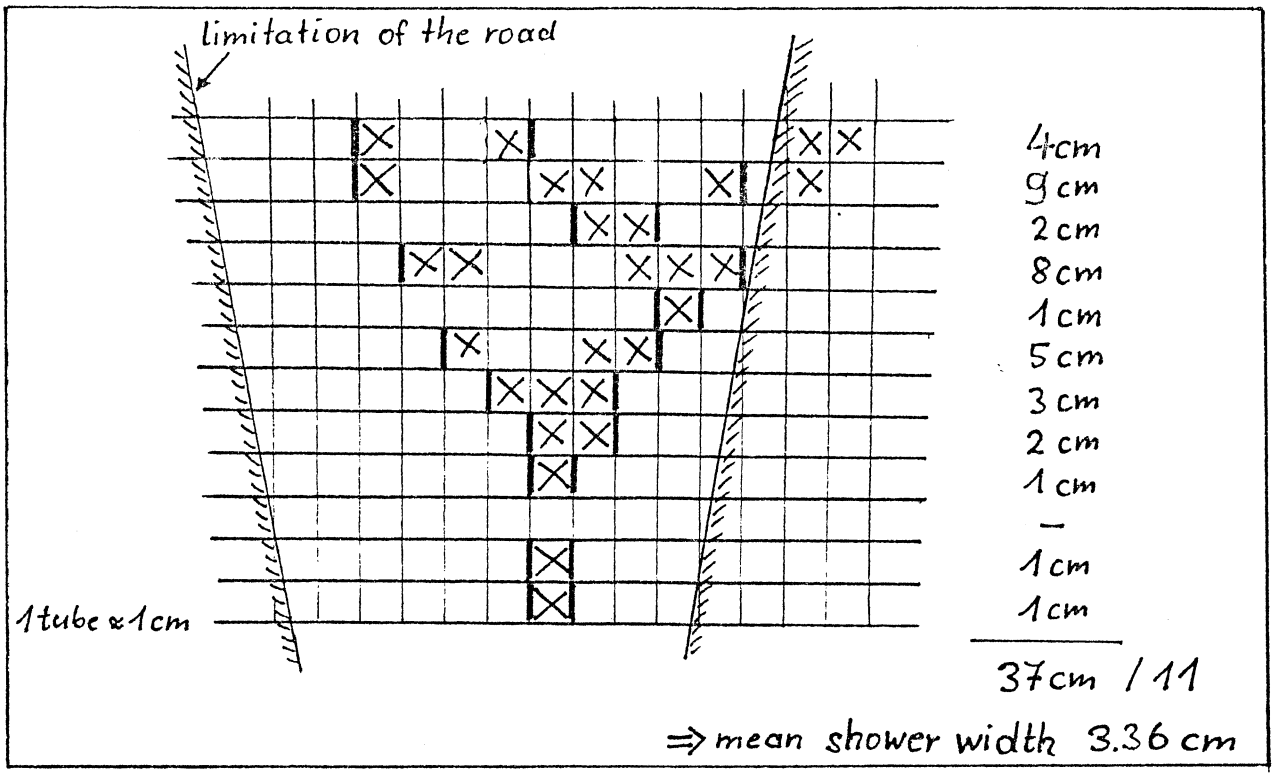
limitation of the road
1 tube ≈ 1 cm
4 cm
9 cm
2 cm
8 cm
1 cm
5 cm
3 cm
2 cm
1 cm
–
1 cm
1 cm
37 cm / 11
⇒ mean shower width 3.36 cm

Fig. 3

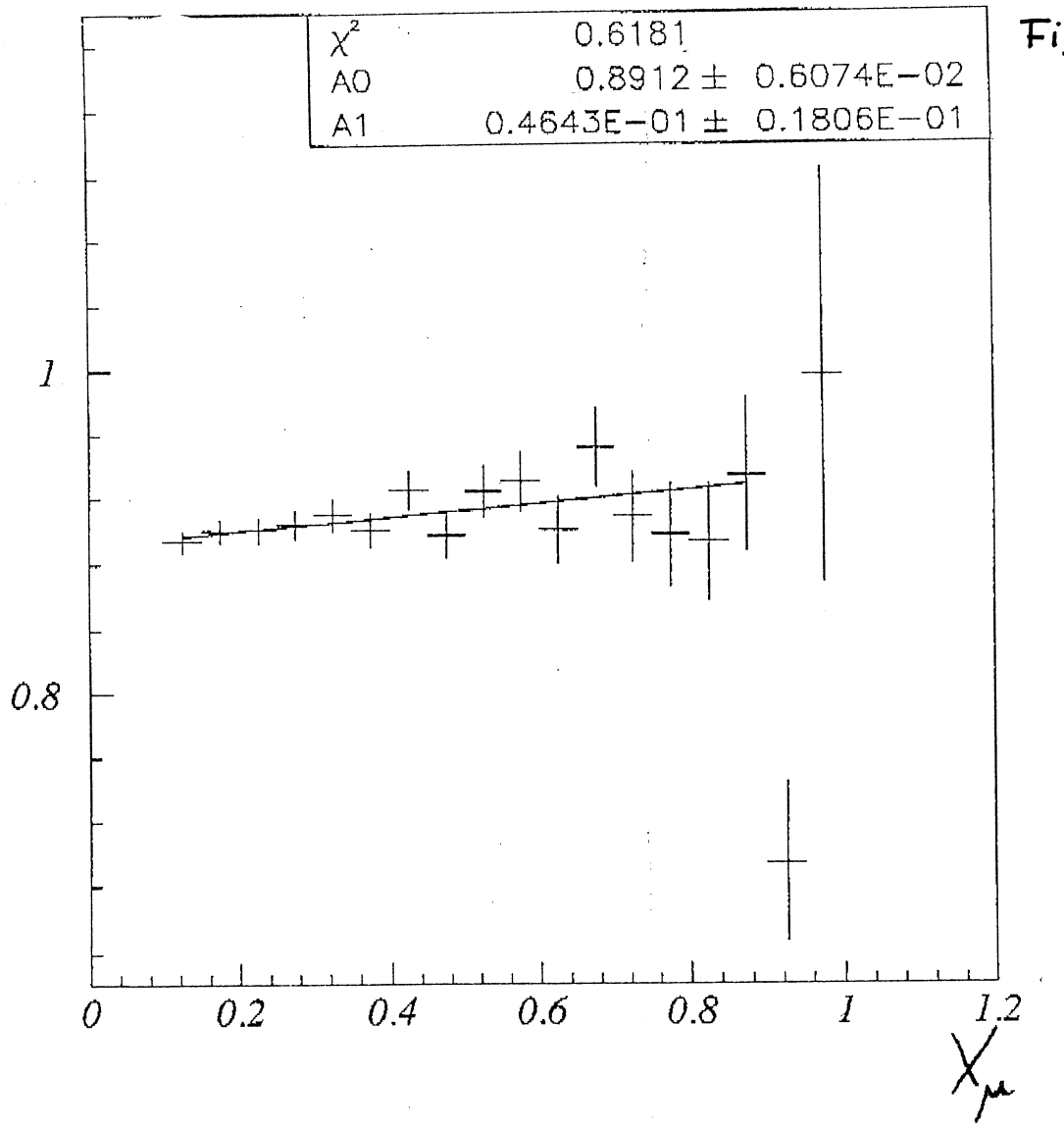
χ² 0.6181
A0 0.8912 ± 0.6074E−02
A1 0.4643E−01 ± 0.1806E−01
1
0.8
0
0.2
0.4
0.6
0.8
1
1.2
X_μ

Fig. 2

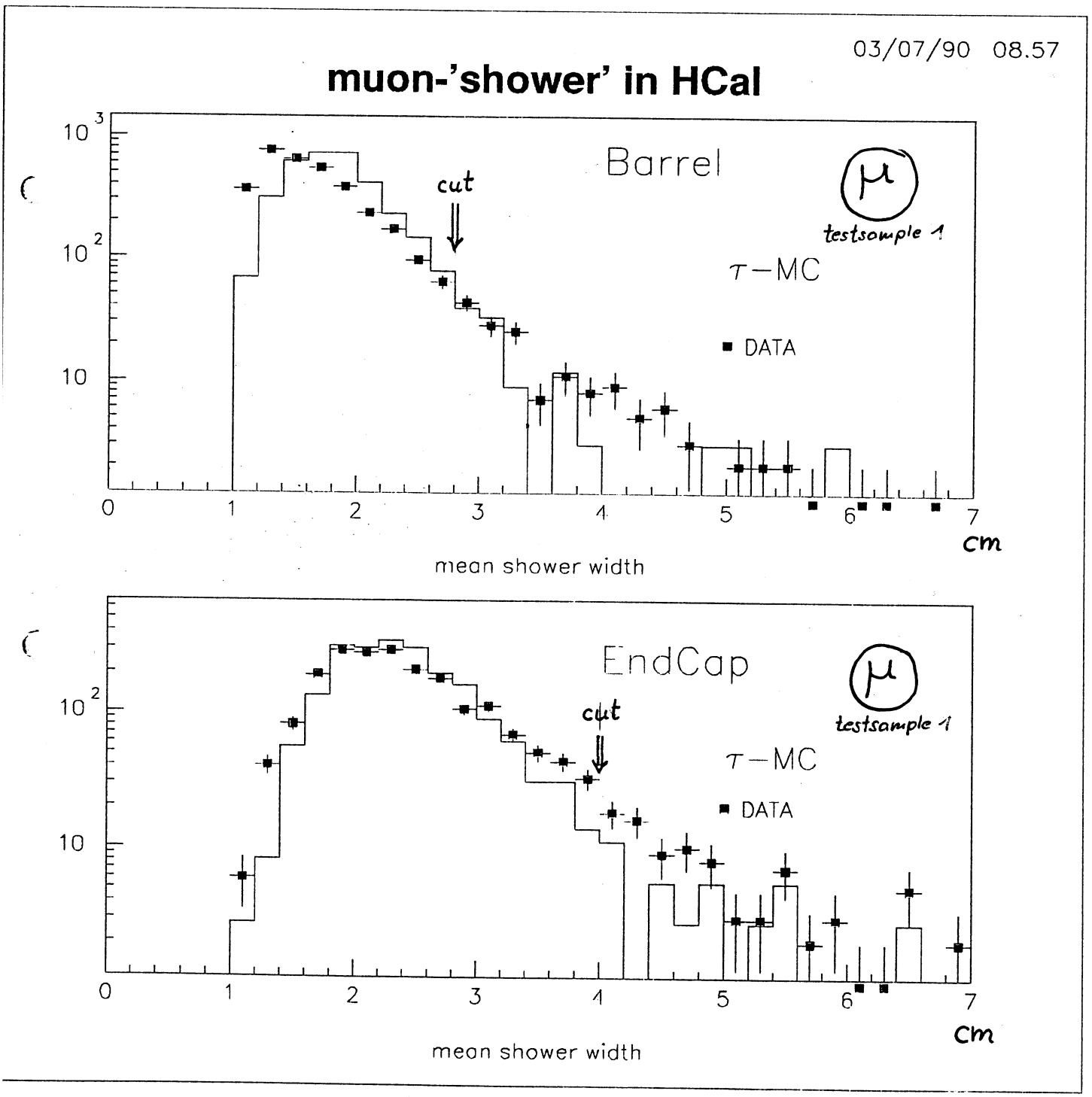
03/07/90 08.57
muon-'shower' in HCal
Barrel
cut
μ
testsample 1
τ−MC
DATA
mean shower width
cm
EndCap
cut
μ
testsample 1
τ−MC
DATA
mean shower width
cm

Fig. 4

17/01/91 14.39

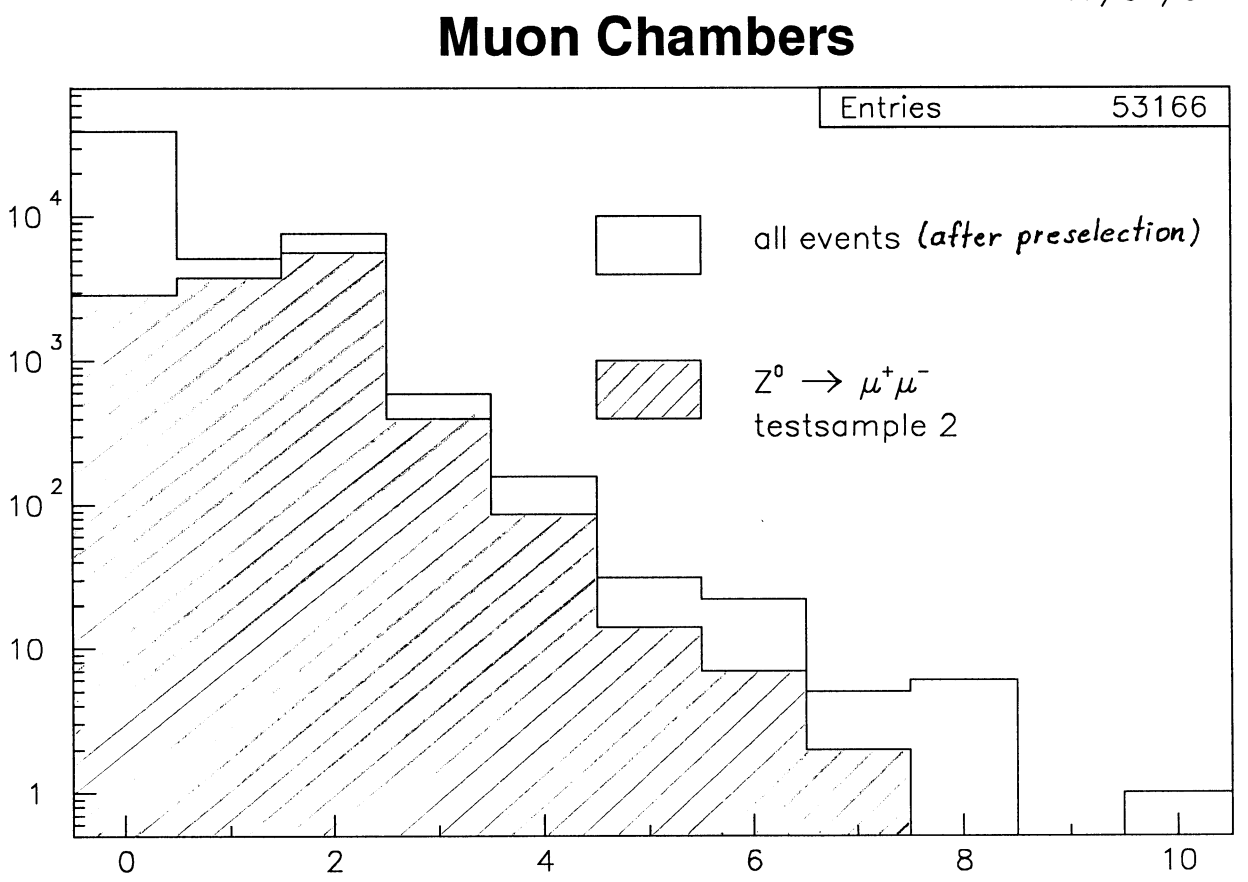

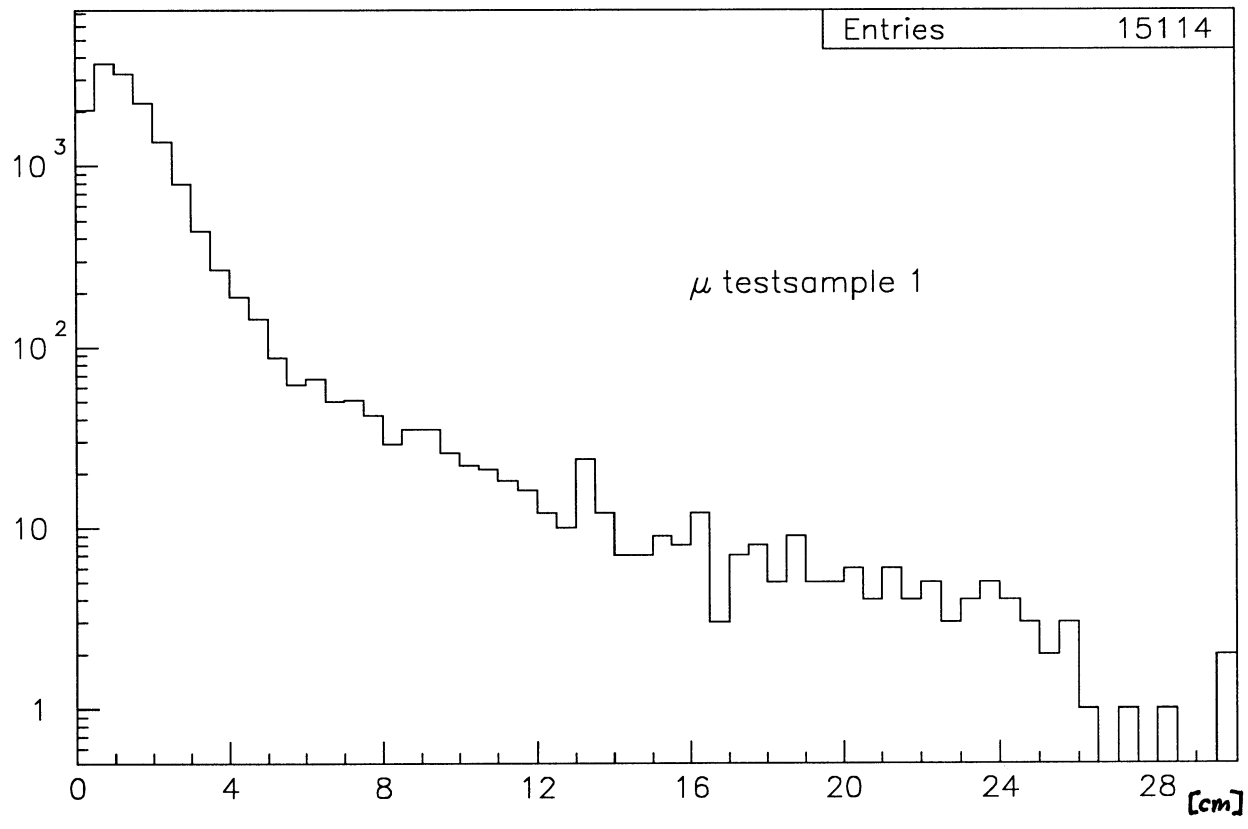

Fig. 5

19/11/90 16.08

IDENTIFICATION EFFICIENCY

Testsample : μ–chamber tagging — isolated tracks associated with at least one hit in a μ–chamber

Identification : penetration ≧ 4 hits

hadron rejection width < 2.8 cm (Ba)

width < 4.0 cm (EC)

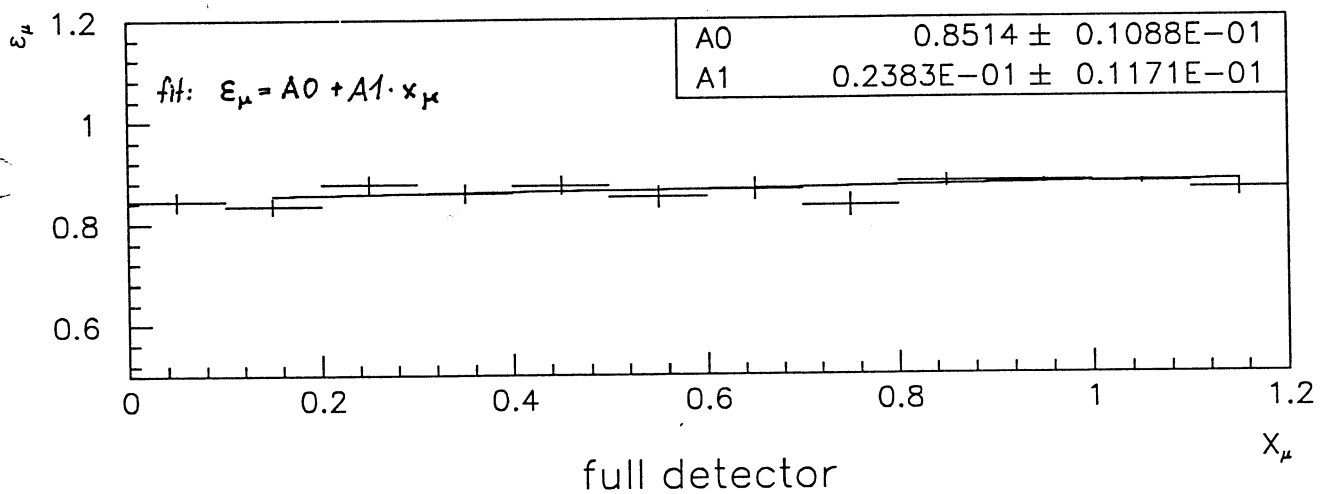

full detector

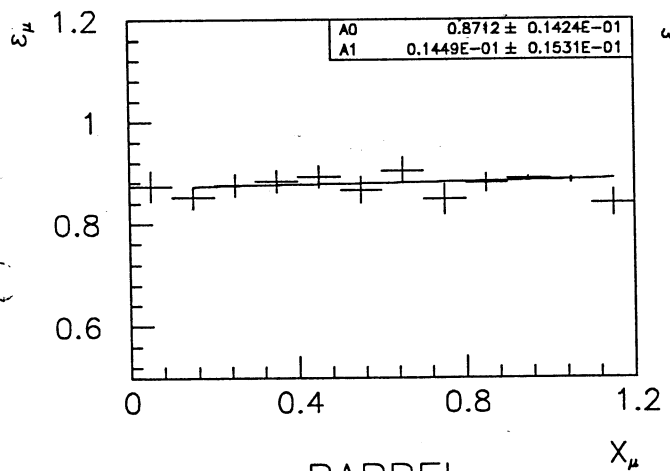

BARREL

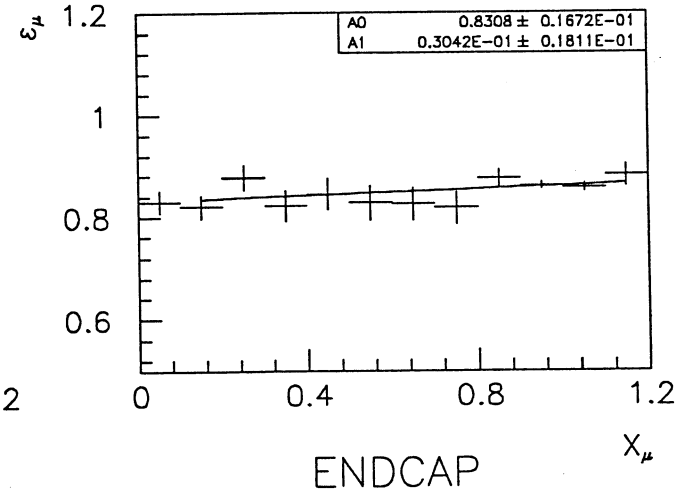

ENDCAP

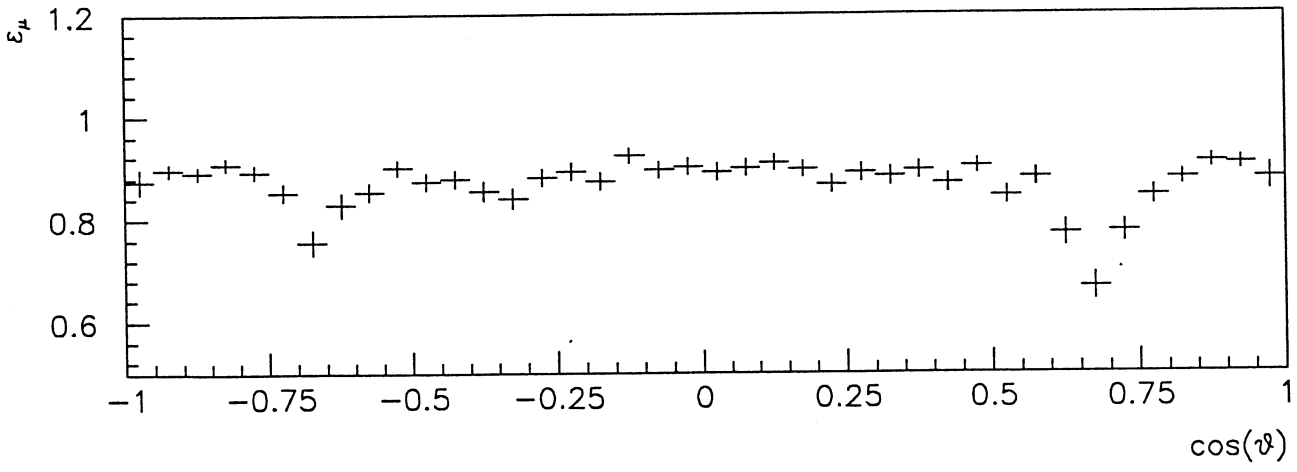

Fig. 6

19/11/90 16.09

PRE-IDENTIFICATION EFFICIENCY

Testsample : μ–chamber tagging — isolated tracks associated with at least one hit in a μ–chamber

Identification : penetration (fired/exp.)planes > 0.2
no hadron rejection

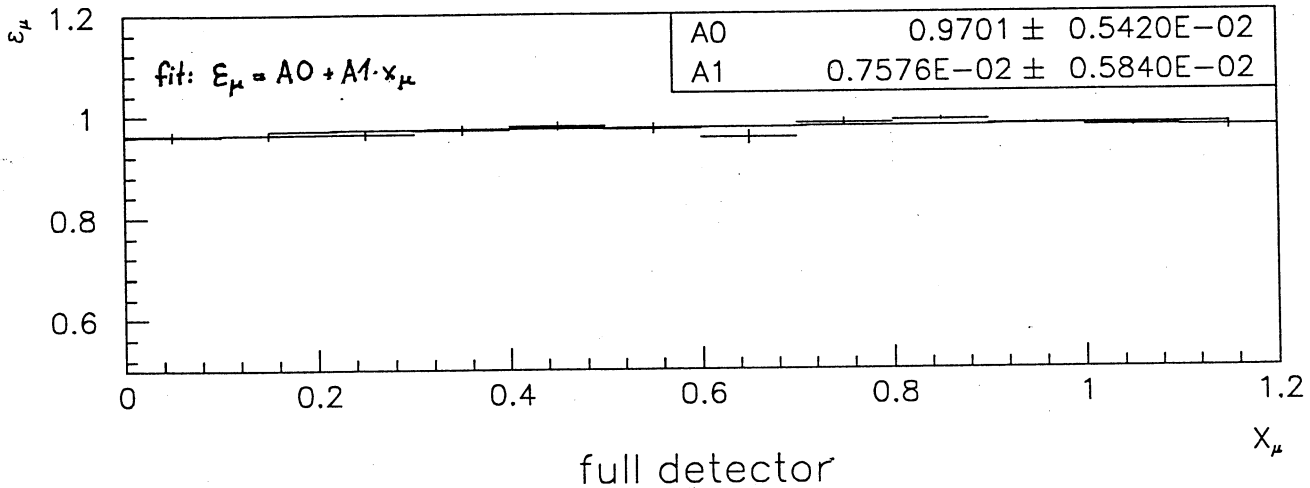

full detector

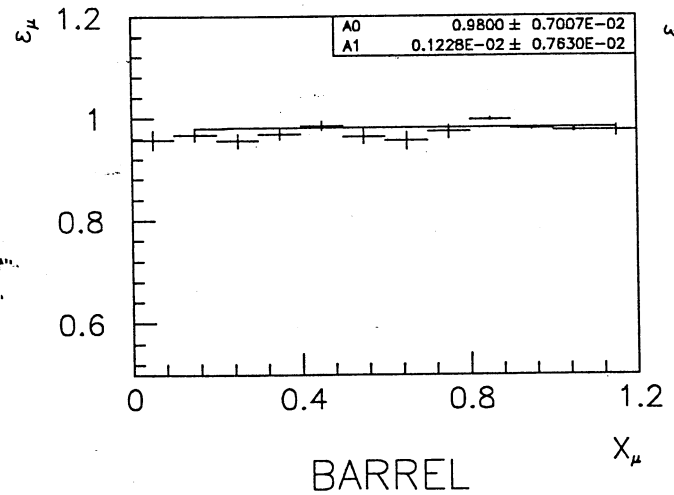

BARREL

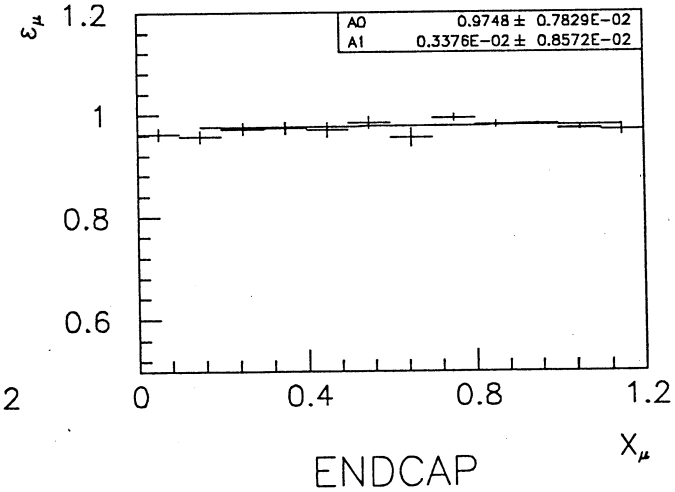

ENDCAP

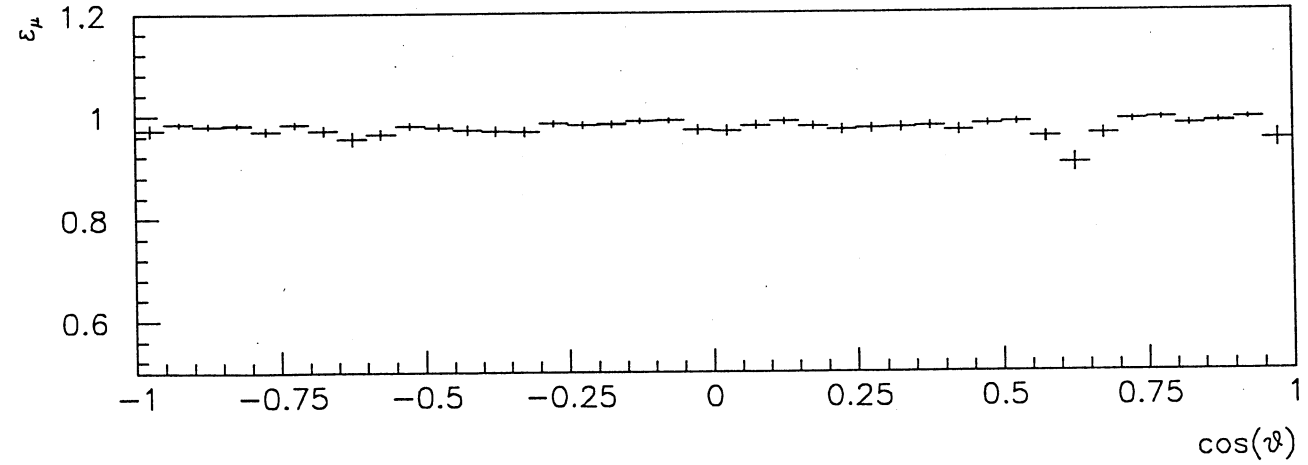

Fig. 7

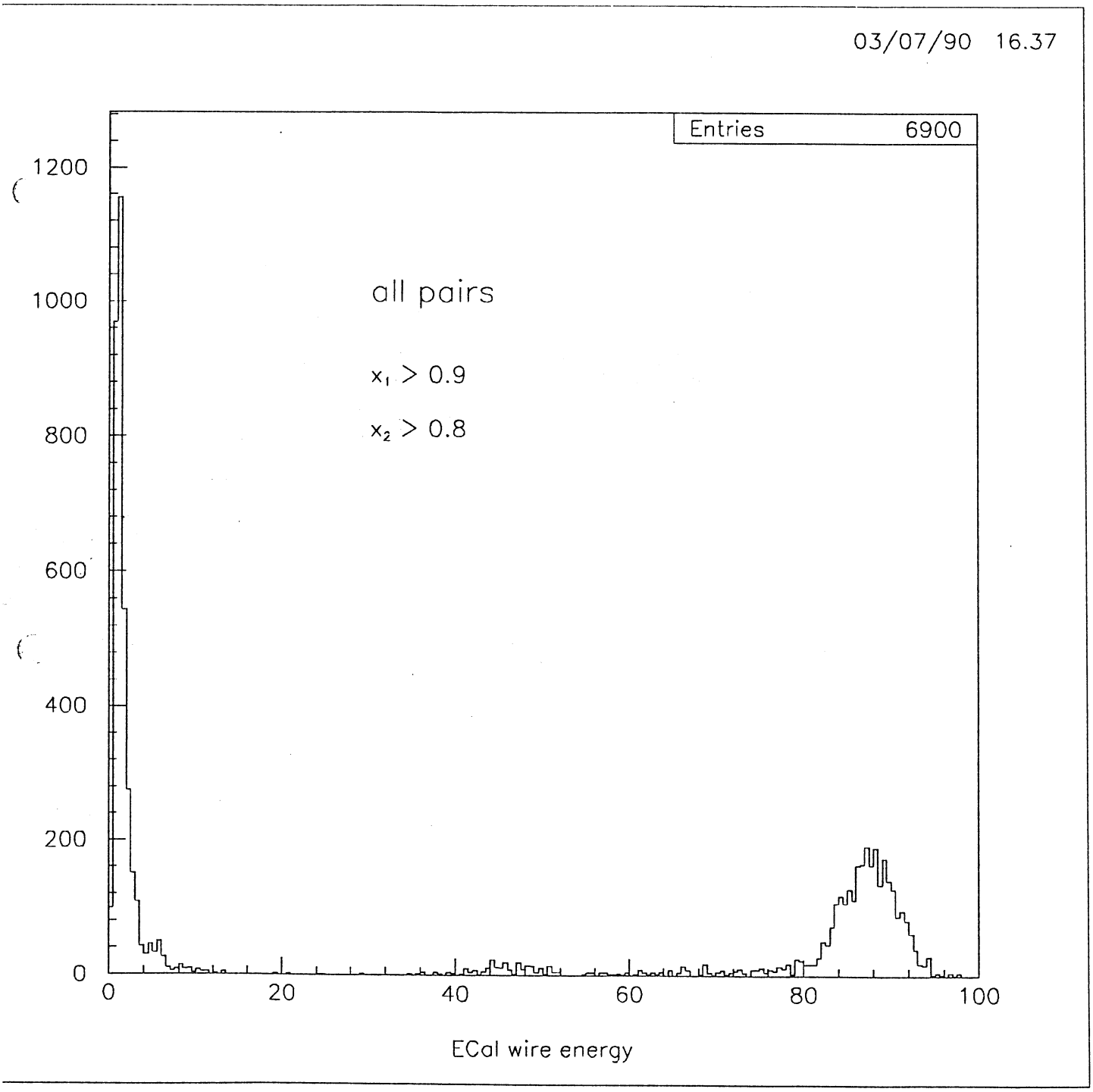
03/07/90 16.37
Entries 6900
all pairs
$x_1 > 0.9$
$x_2 > 0.8$
1200
1000
800
600
400
200
0
0
20
40
60
80
100
ECal wire energy

Fig. 8

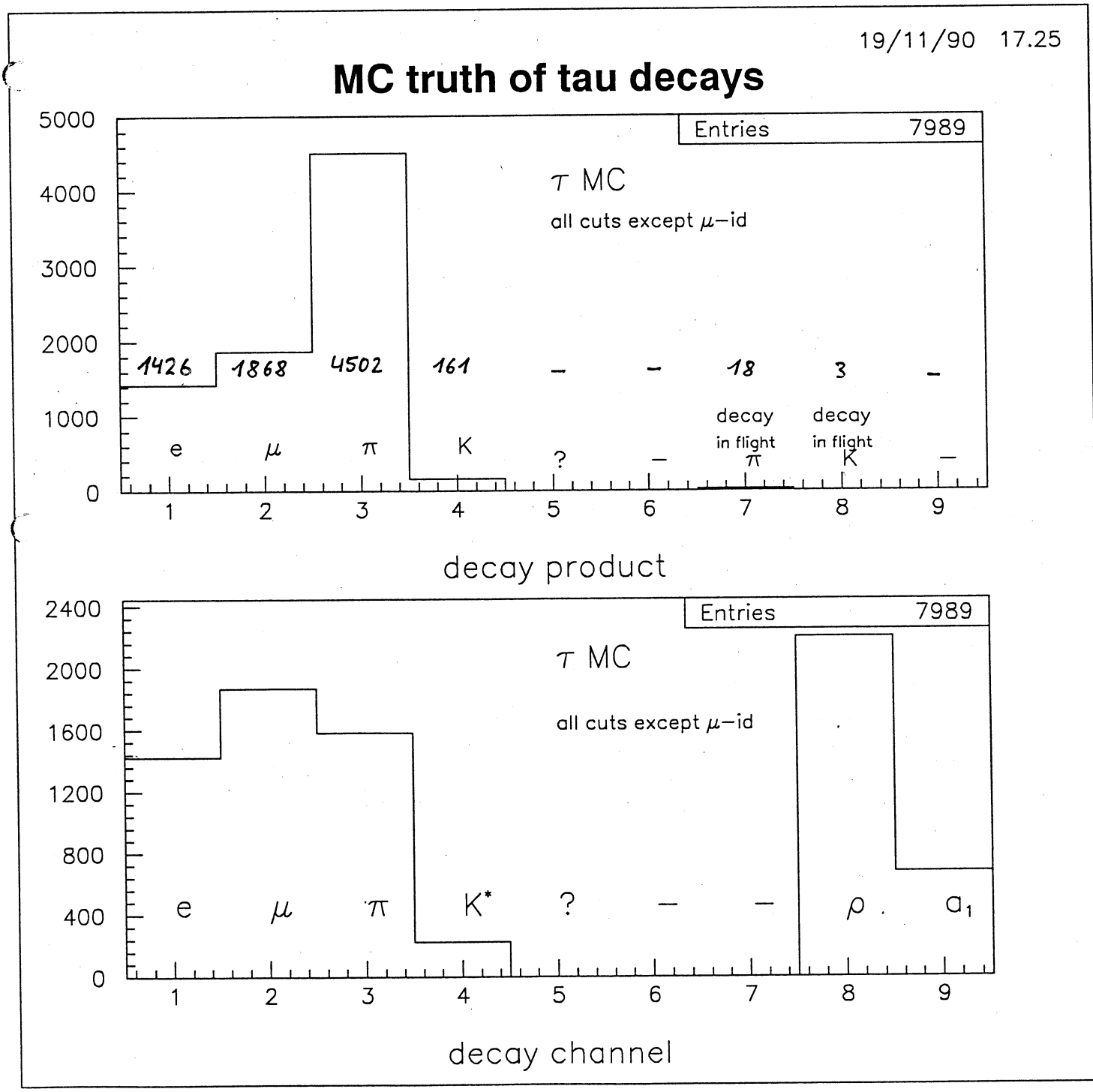
19/11/90 17.25
MC truth of tau decays
Entries 7989
τ MC
all cuts except μ–id
1426
1868
4502
161
–
–
18
3
–
e
μ
π
K
?
–
decay in flight π
decay in flight K
–
decay product
Entries 7989
τ MC
all cuts except μ–id
e
μ
π
K*
?
–
–
ρ
a1
decay channel

Fig. 9a

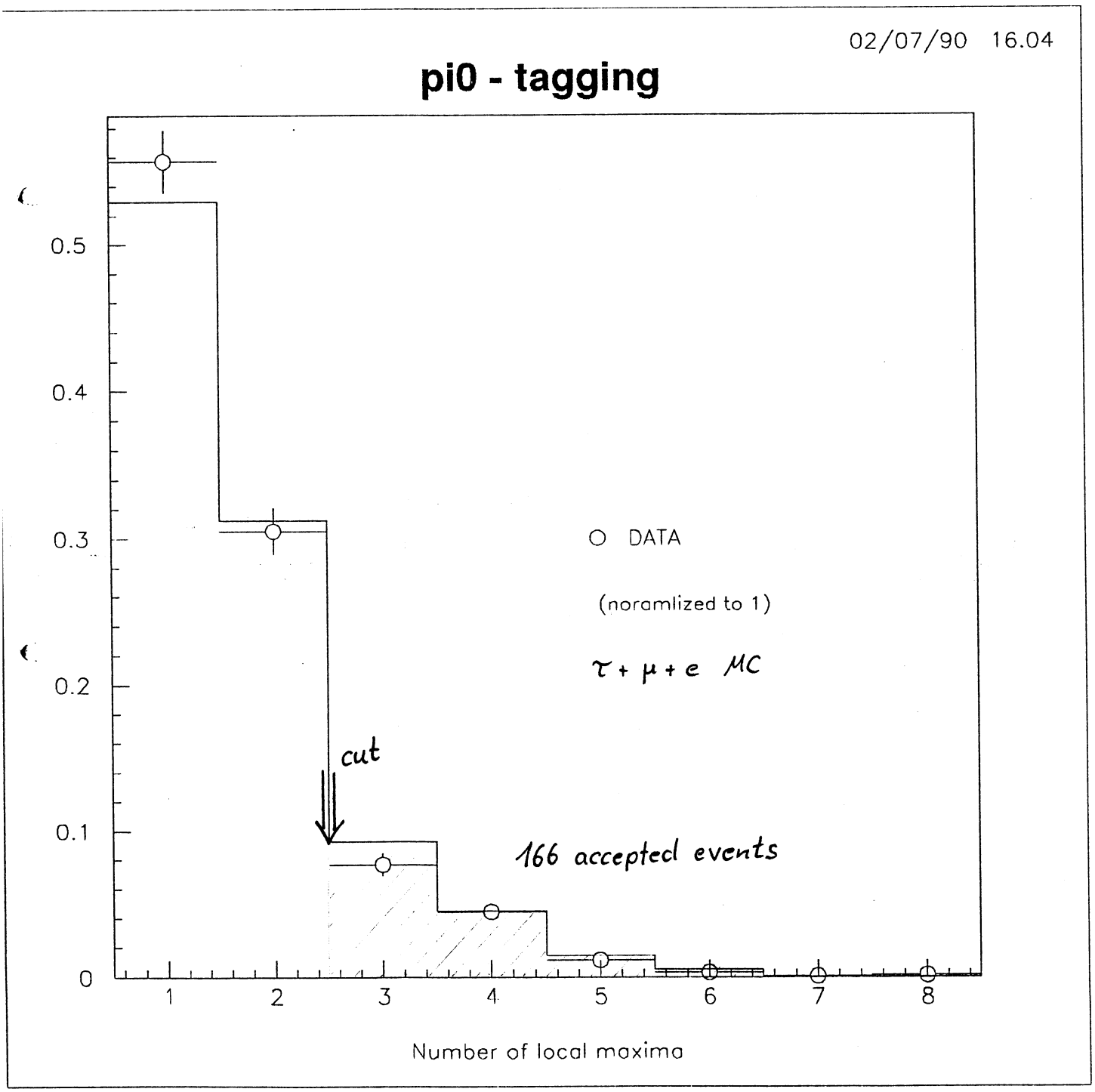
02/07/90 16.04
pi0 - tagging
0.5
0.4
0.3
0.2
0.1
0
DATA
(noramlized to 1)
τ + μ + e MC
cut
166 accepted events
1
2
3
4
5
6
7
8
Number of local maxima

Fig. 9b

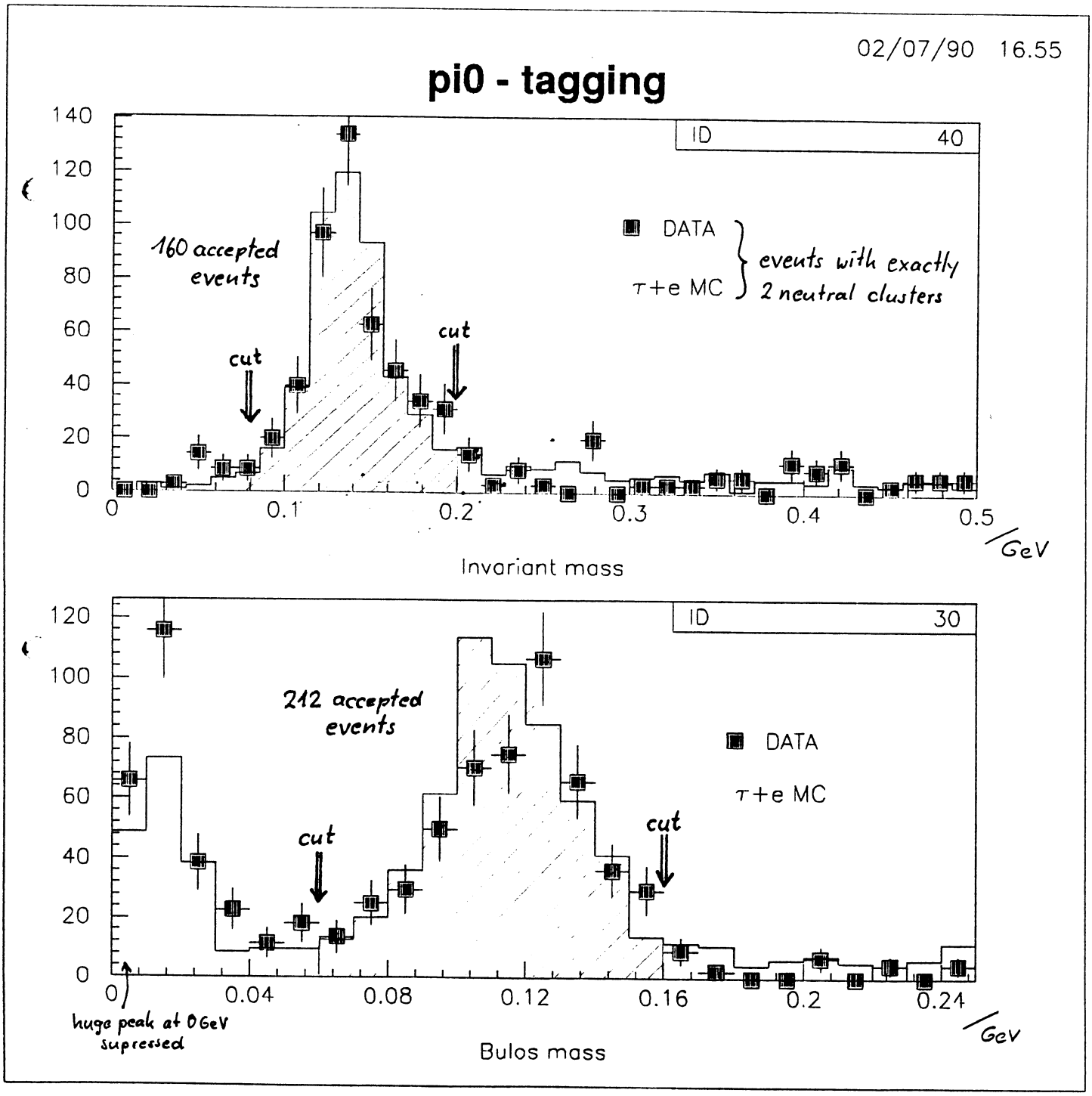
02/07/90 16.55
pi0 - tagging
ID 40
DATA
τ+e MC
events with exactly 2 neutral clusters
160 accepted events
cut
cut
140
120
100
80
60
40
20
0
0
0.1
0.2
0.3
0.4
0.5
GeV
Invariant mass
ID 30
212 accepted events
DATA
τ+e MC
cut
cut
120
100
80
60
40
20
0
0
0.04
0.08
0.12
0.16
0.2
0.24
GeV
huge peak at 0 GeV supressed
Bulos mass

Fig. 10

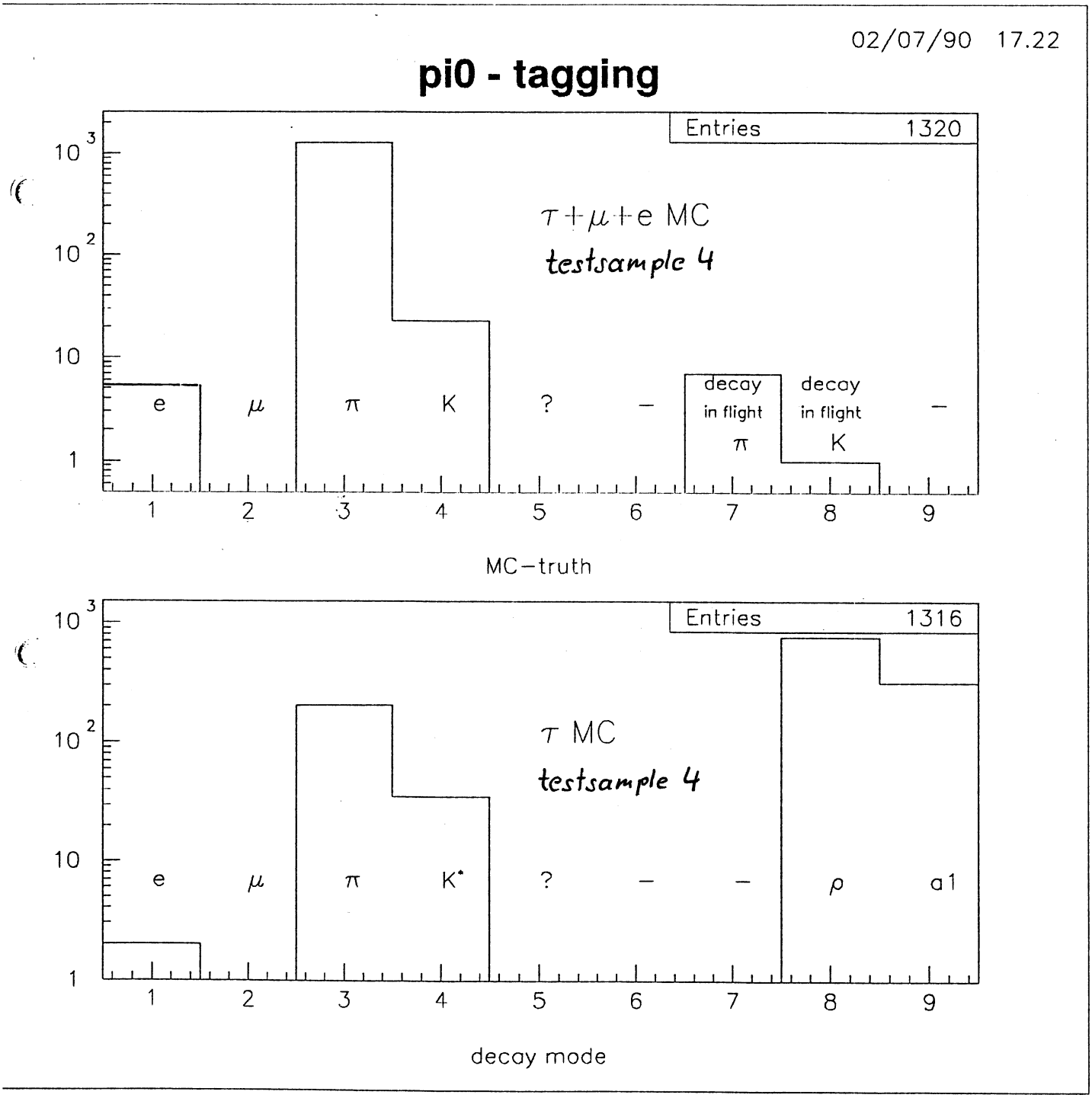
02/07/90 17.22
pi0 - tagging
Entries 1320
τ+μ+e MC
testsample 4
e
μ
π
K
?
–
decay in flight π
decay in flight K
–
MC–truth
Entries 1316
τ MC
testsample 4
e
μ
π
K*
?
–
–
ρ
a1
decay mode

Fig. 11

18/01/91 16.05

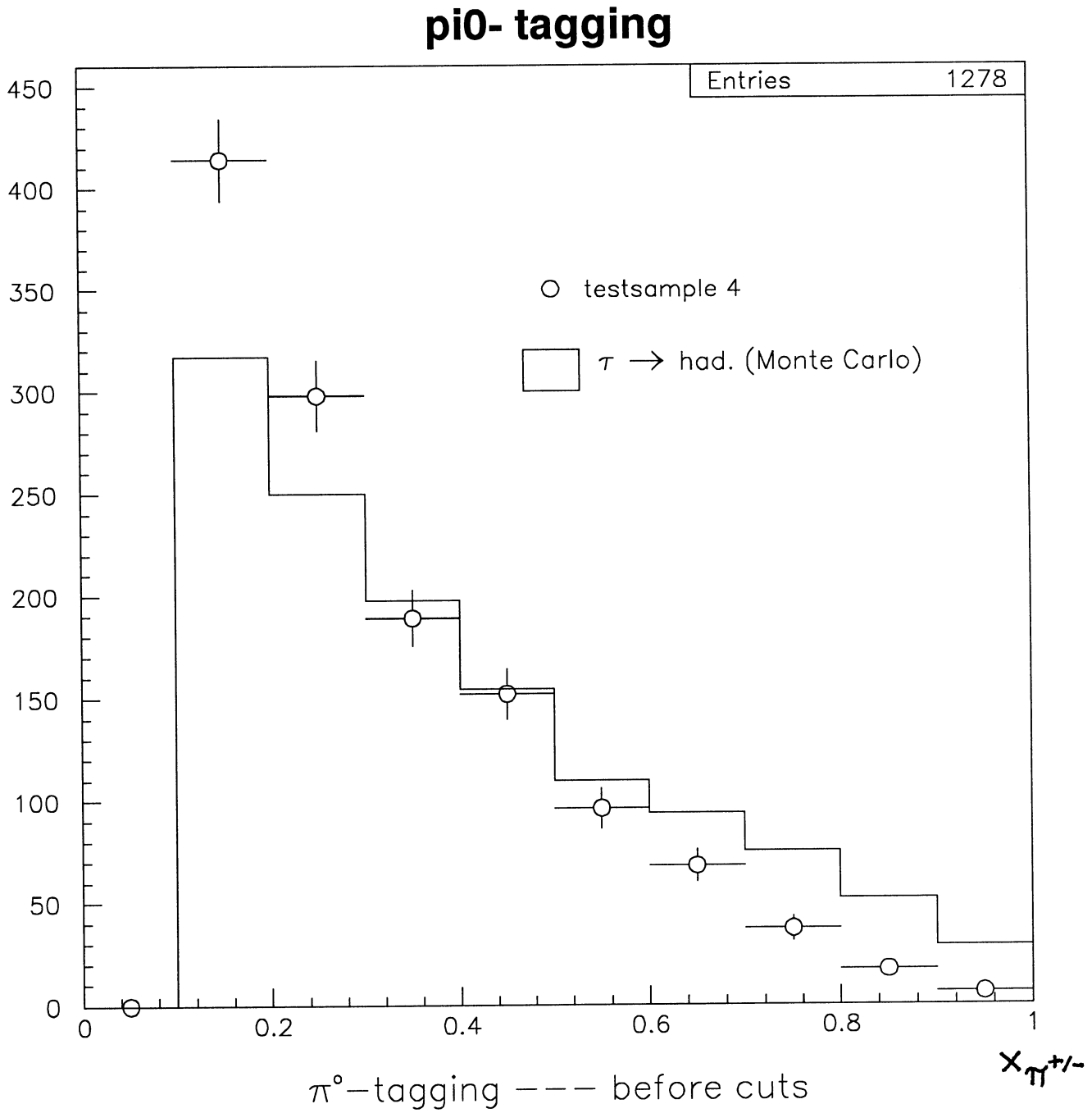

Fig. 12a

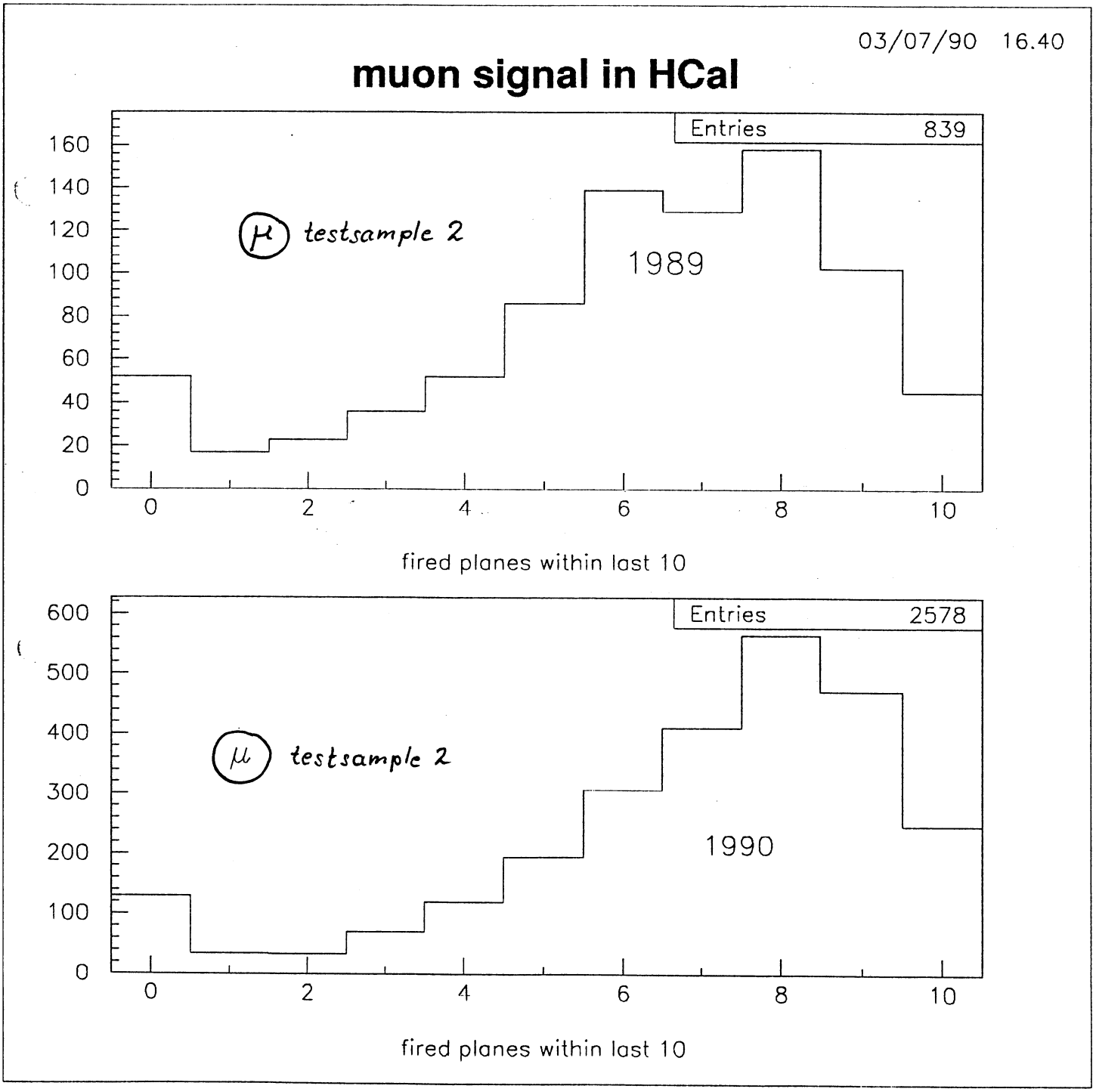
03/07/90 16.40
muon signal in HCal
Entries 839
μ testsample 2
1989
160
140
120
100
80
60
40
20
0
0
2
4
6
8
10
fired planes within last 10
Entries 2578
μ testsample 2
1990
600
500
400
300
200
100
0
0
2
4
6
8
10
fired planes within last 10

Fig. 12 b

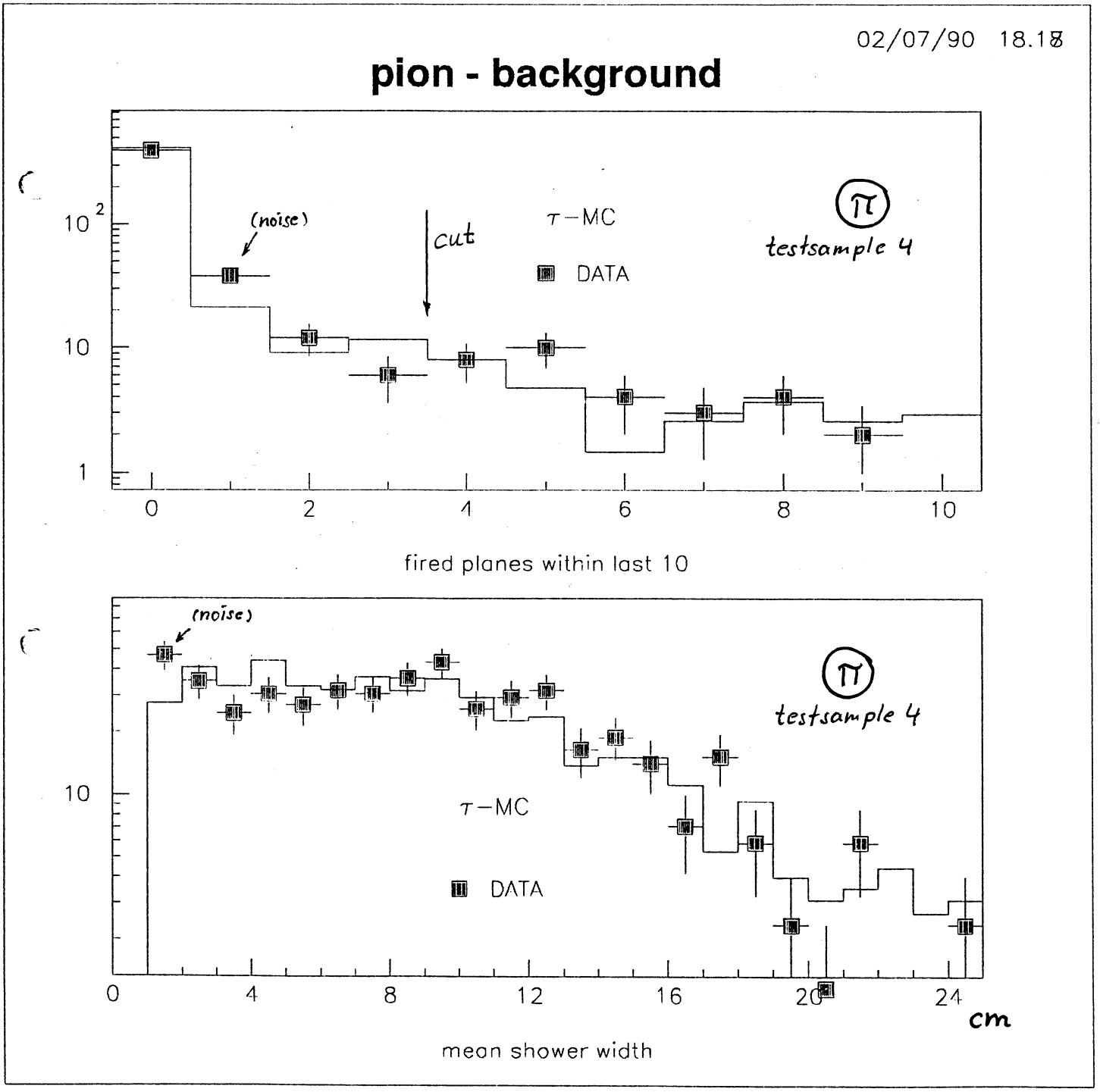
02/07/90 18.18
pion - background
10 2
10
1
(noise)
cut
τ−MC
DATA
π
testsample 4
0
2
4
6
8
10
fired planes within last 10
(noise)
10
τ−MC
DATA
π
testsample 4
0
4
8
12
16
20
24
cm
mean shower width

Fig 13

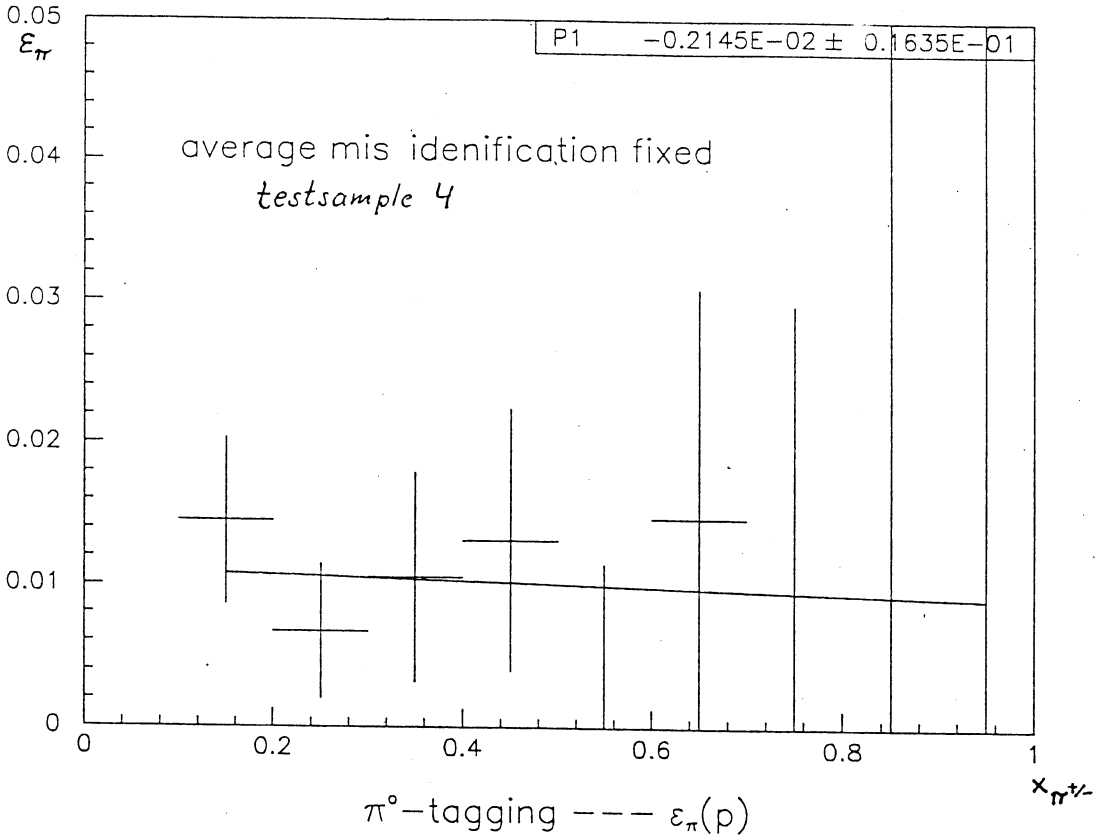

π°−tagging −−− $\varepsilon_\pi(p)$

Fig. 14

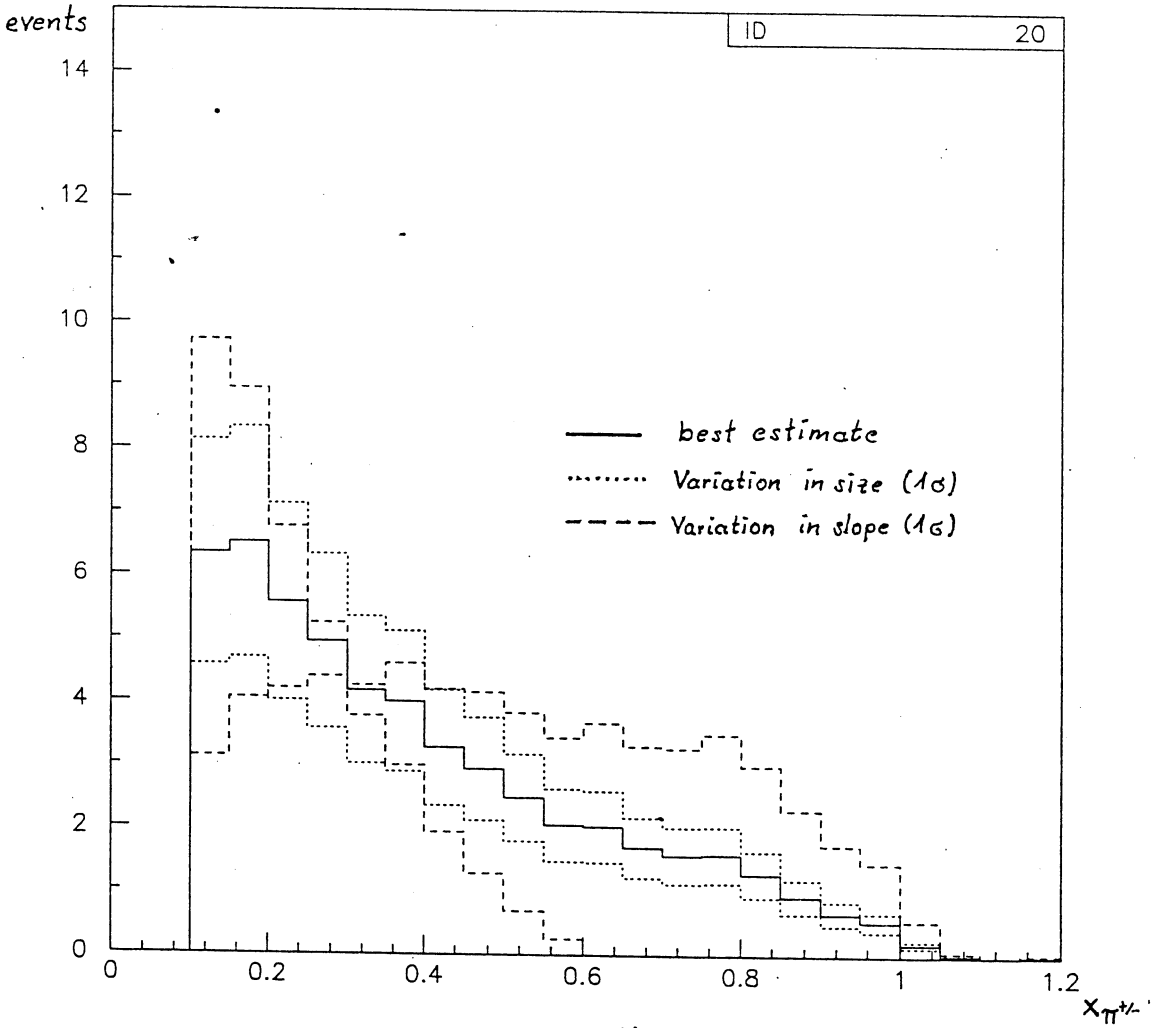

π−correction A

Fig. 15

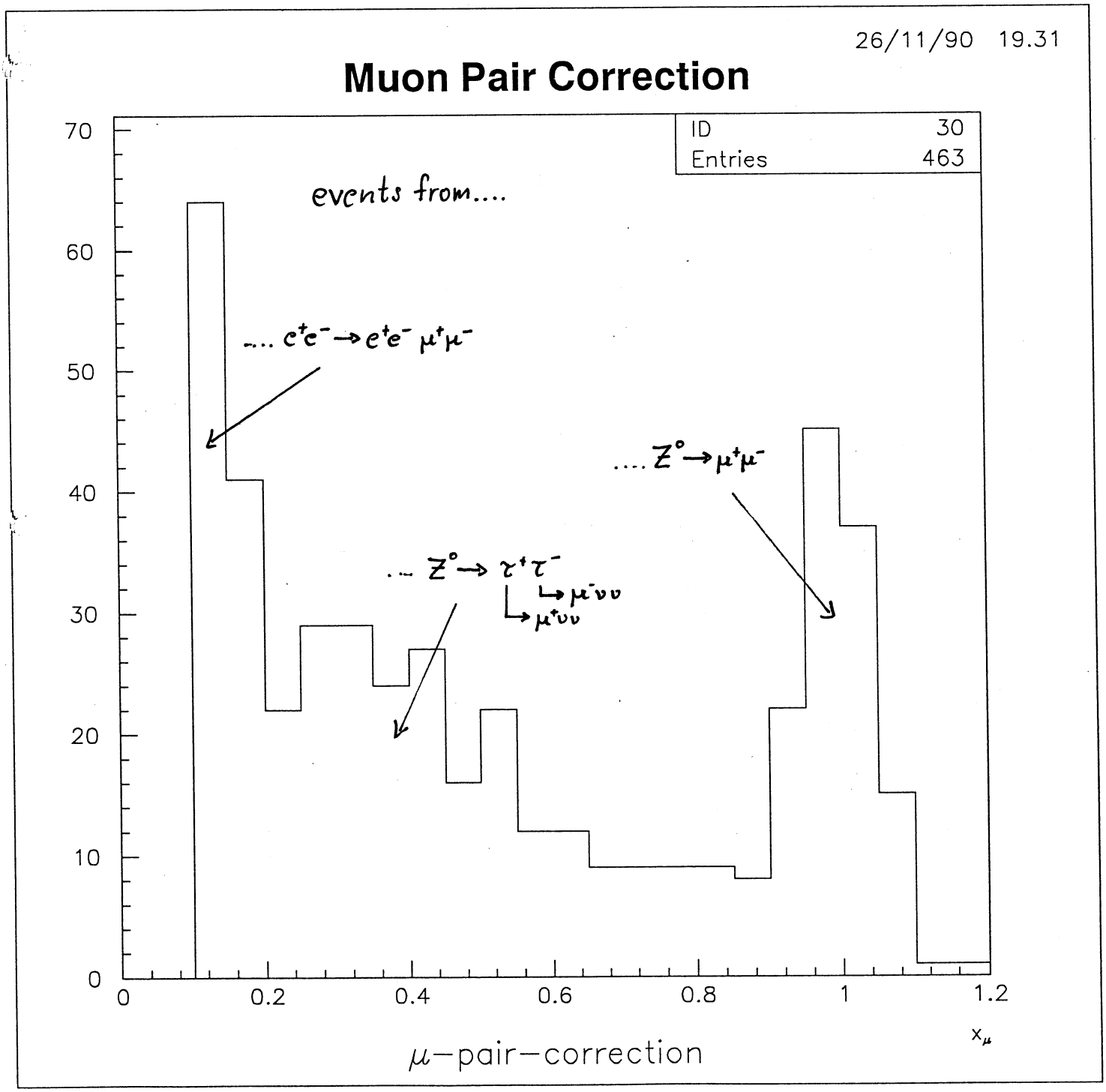
26/11/90 19.31
Muon Pair Correction
ID 30
Entries 463
events from....
.... $e^+e^- \to e^+e^- \mu^+\mu^-$
.... $Z^0 \to \mu^+\mu^-$
... $Z^0 \to \tau^+\tau^-$
$\to \mu^-\nu\nu$
$\to \mu^+\nu\nu$
70
60
50
40
30
20
10
0
0
0.2
0.4
0.6
0.8
1
1.2
x_μ
μ–pair–correction

Fig. 16

21/01/91 18.23

2 PHOTON BACKGROUND

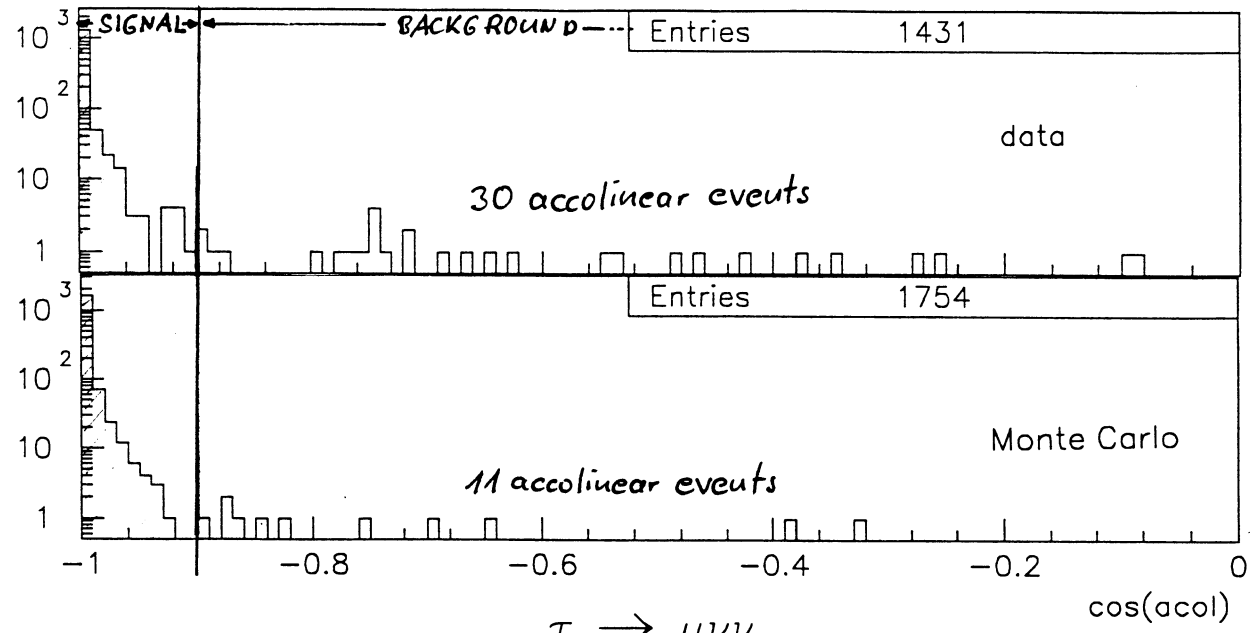

$\tau \rightarrow \mu\nu\nu$

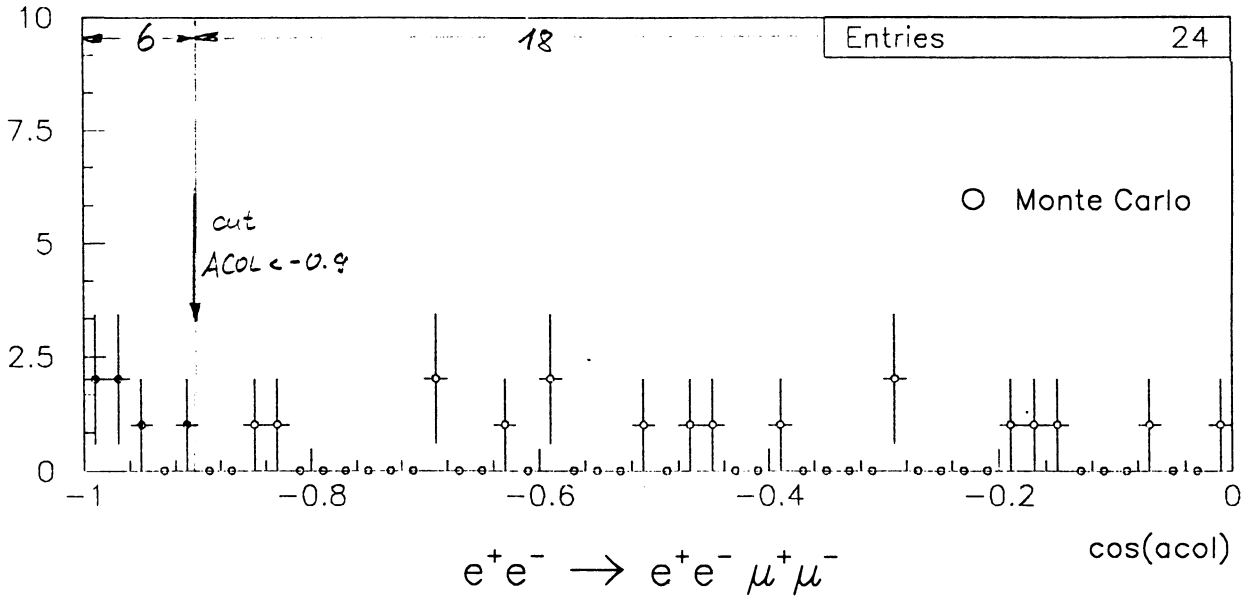

$e^+e^- \rightarrow e^+e^- \mu^+\mu^-$

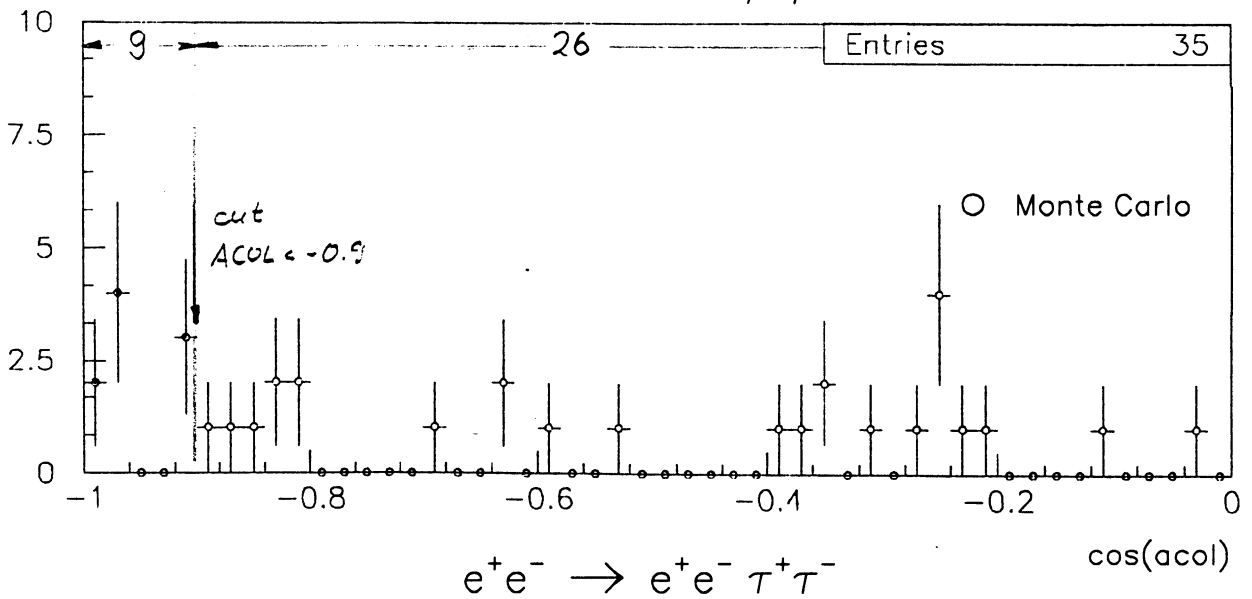

$e^+e^- \rightarrow e^+e^- \tau^+\tau^-$

Fig. 17

21/01/91 20.17

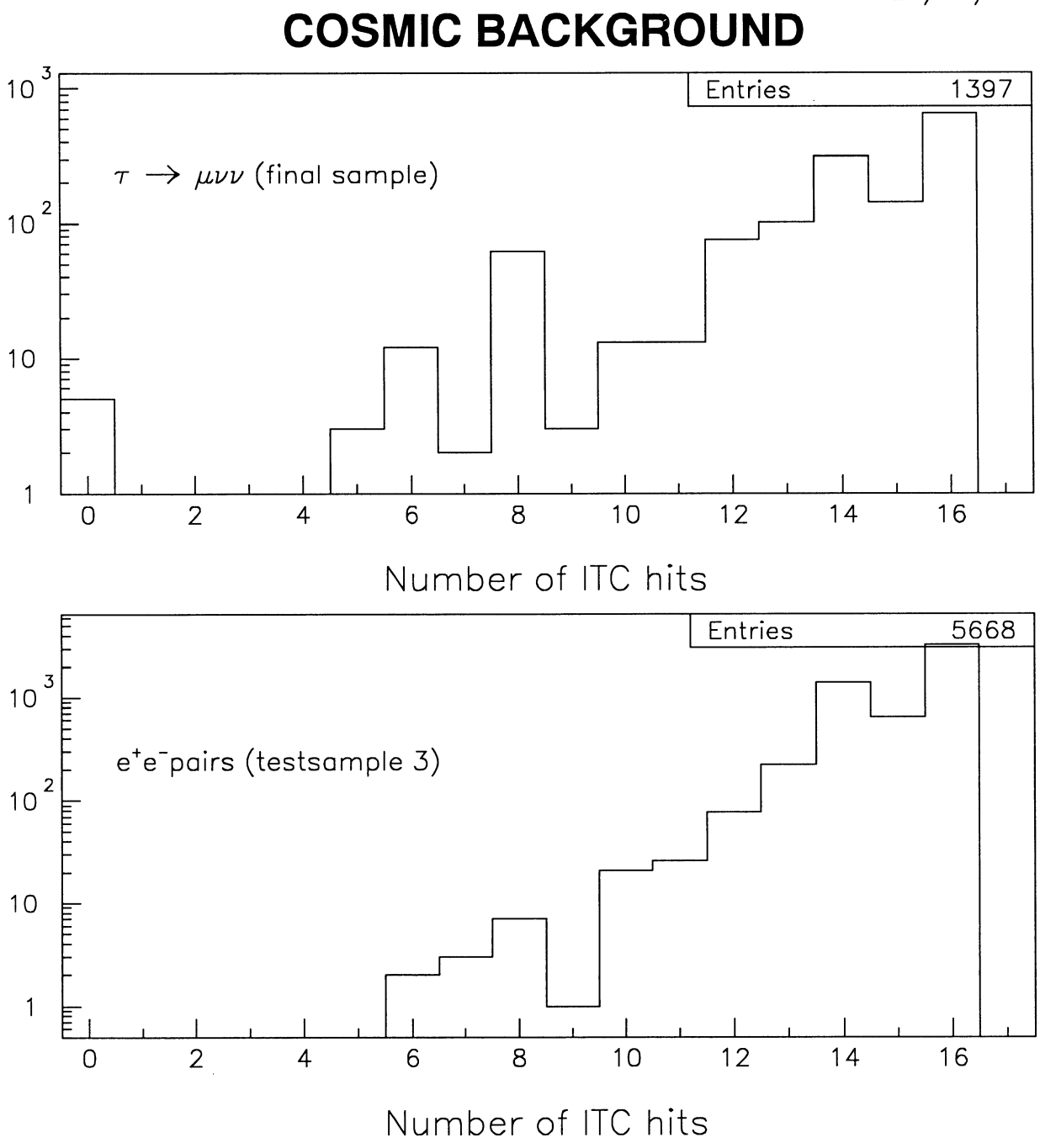

Fig. 18

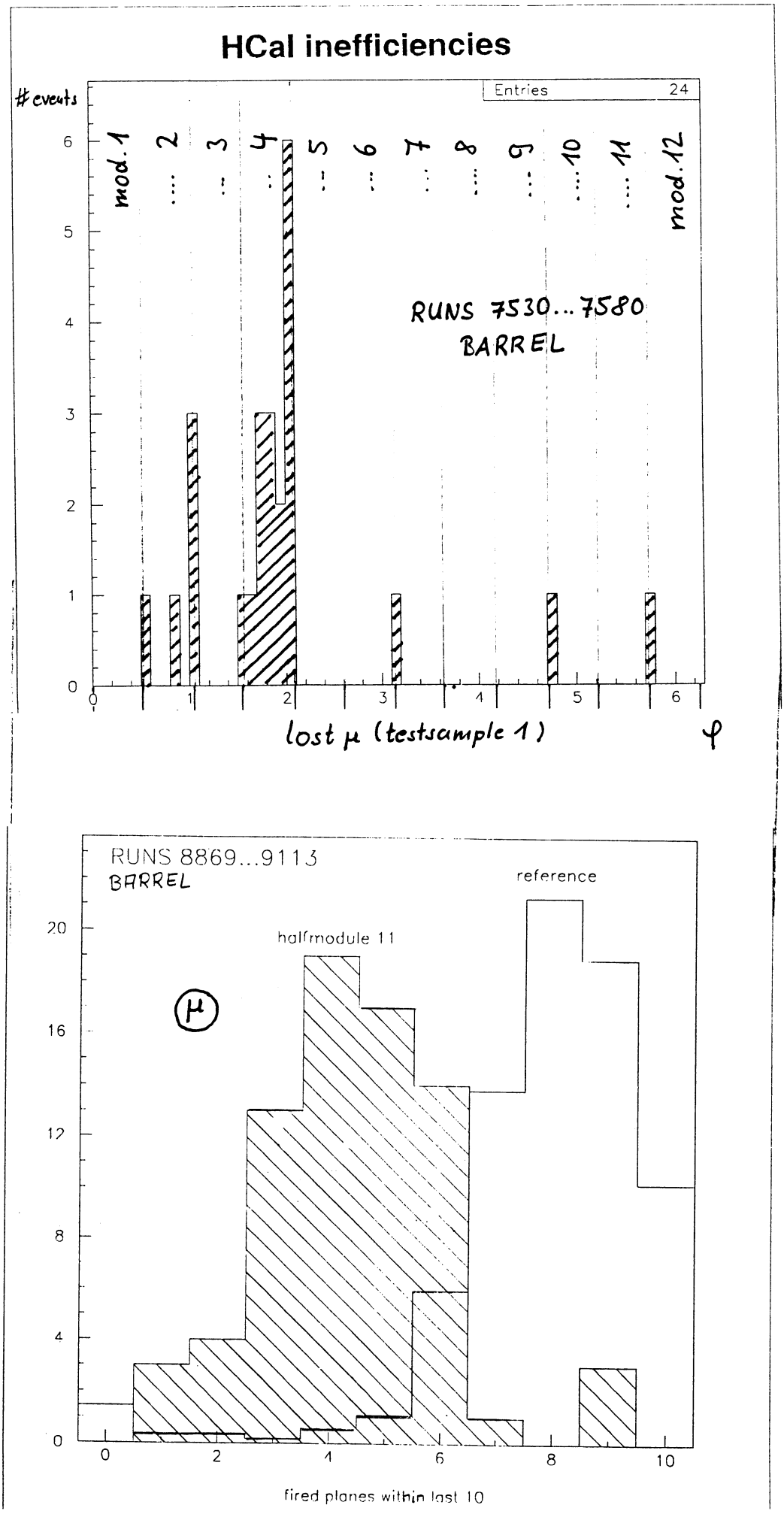
HCal inefficiencies
events
Entries 24
mod. 1
2
3
4
5
6
7
8
9
10
11
mod. 12
RUNS 7530...7580
BARREL
lost μ (testsample 1)
φ
RUNS 8869...9113
BARREL
reference
halfmodule 11
μ
fired planes within last 10

Fig 19

29/08/90 12.36

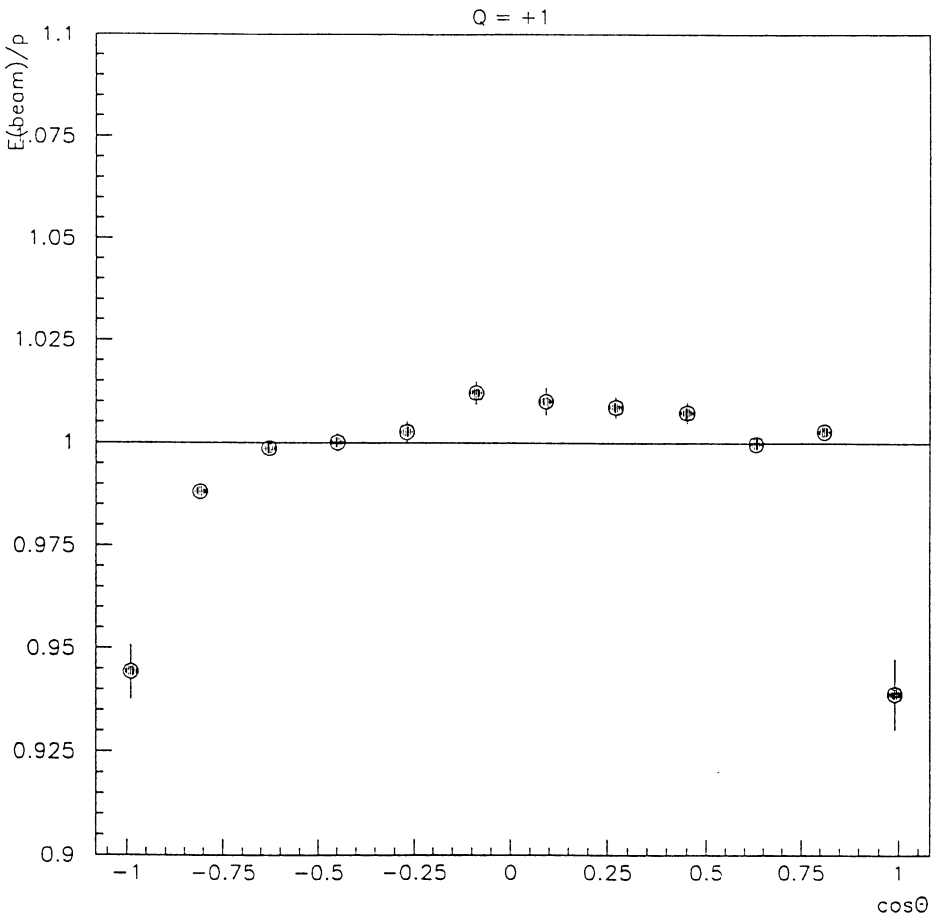

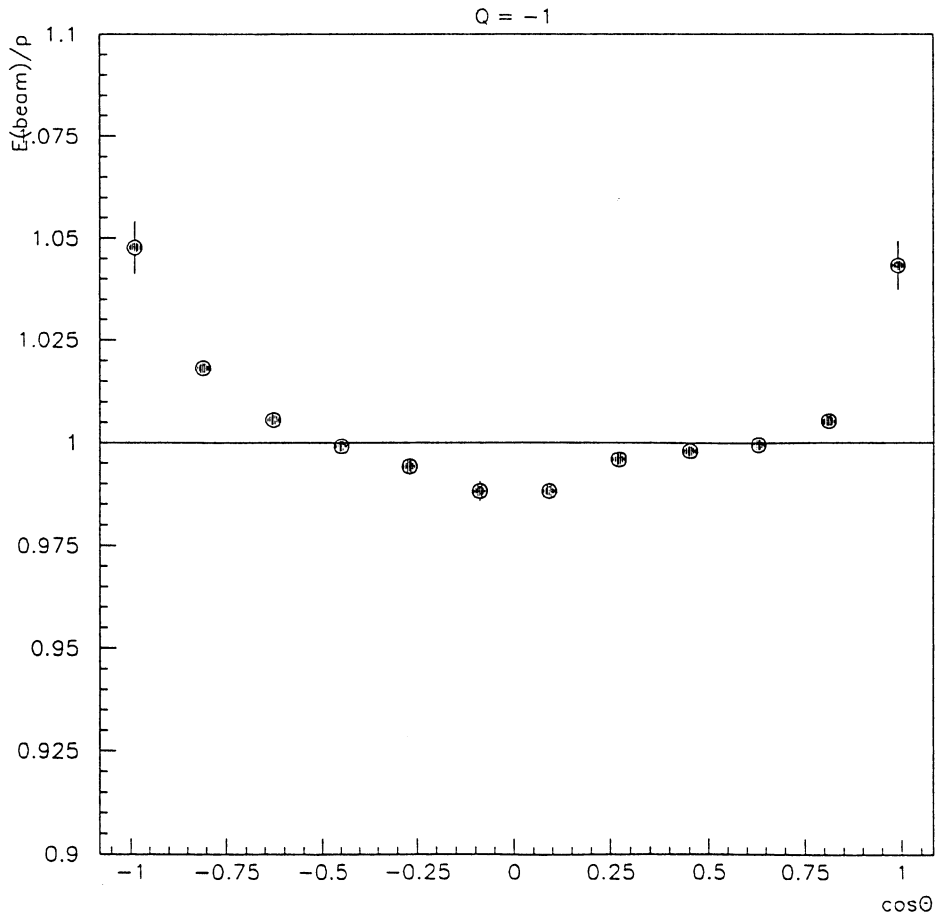

21/11/90 10.28

Correction of TPC Scale

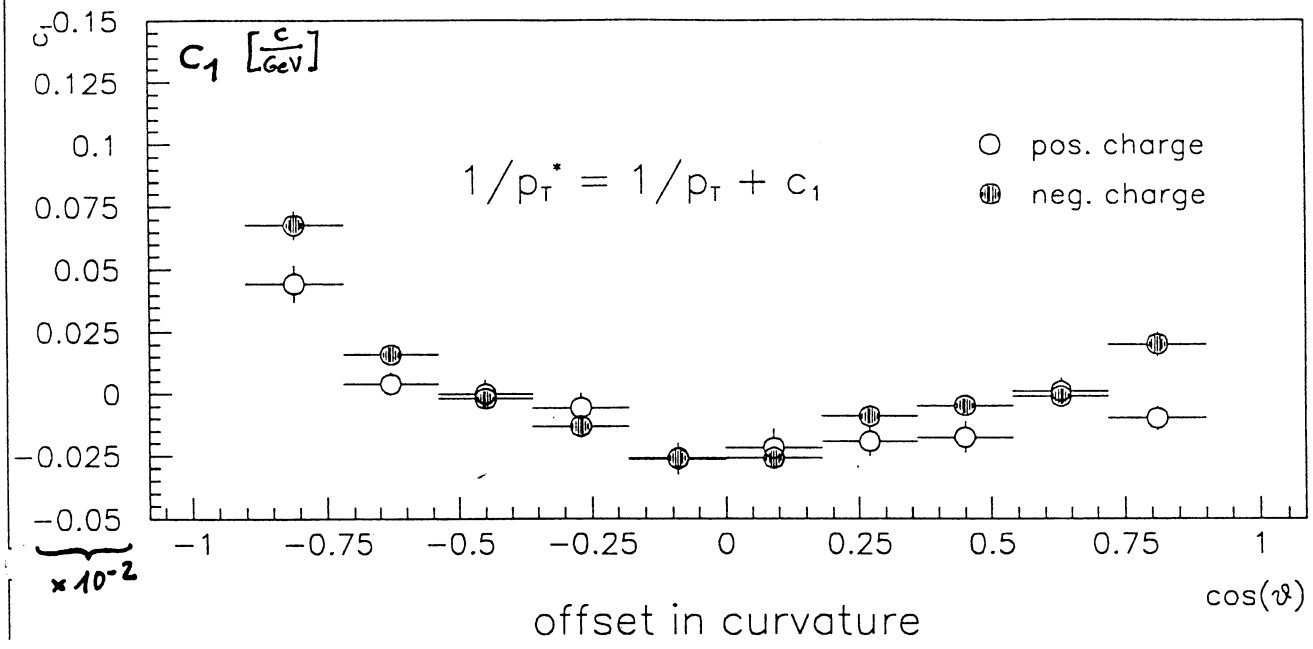

offset in curvature

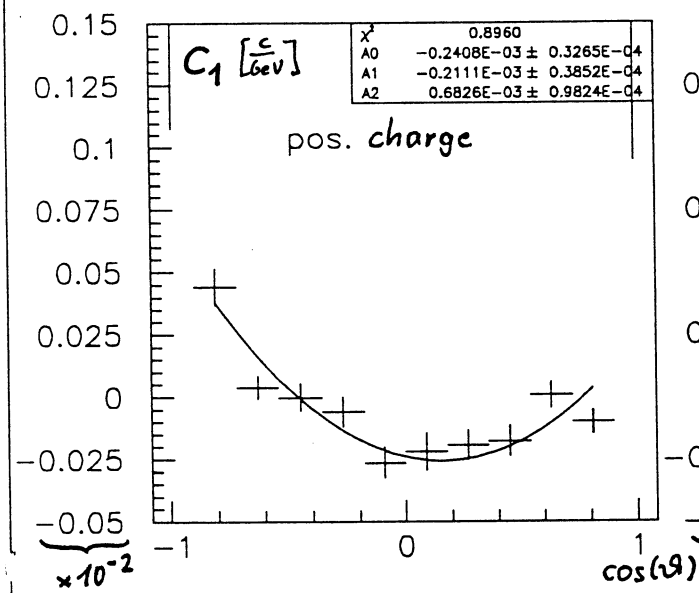

offset in curvature

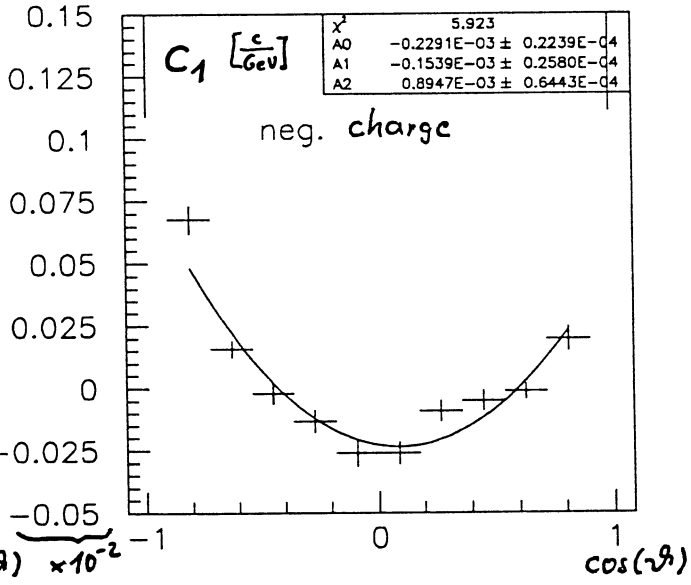

offset in curvature

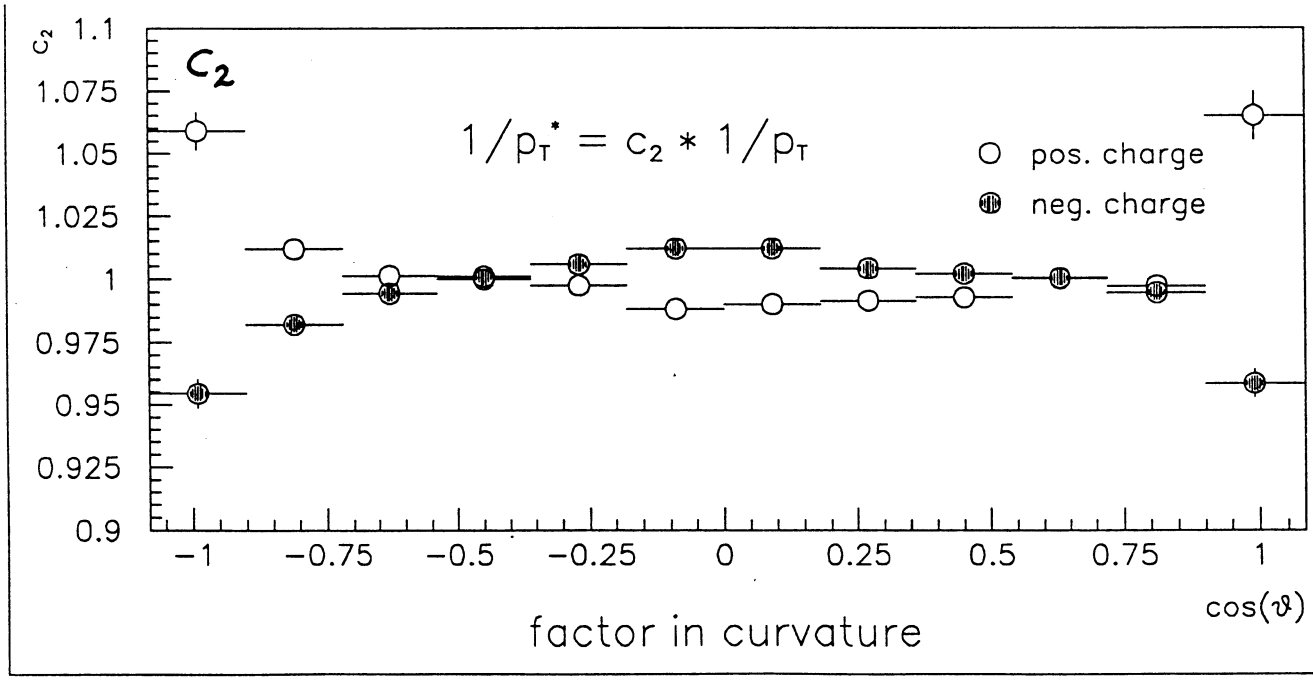

factor in curvature

Fig. 21

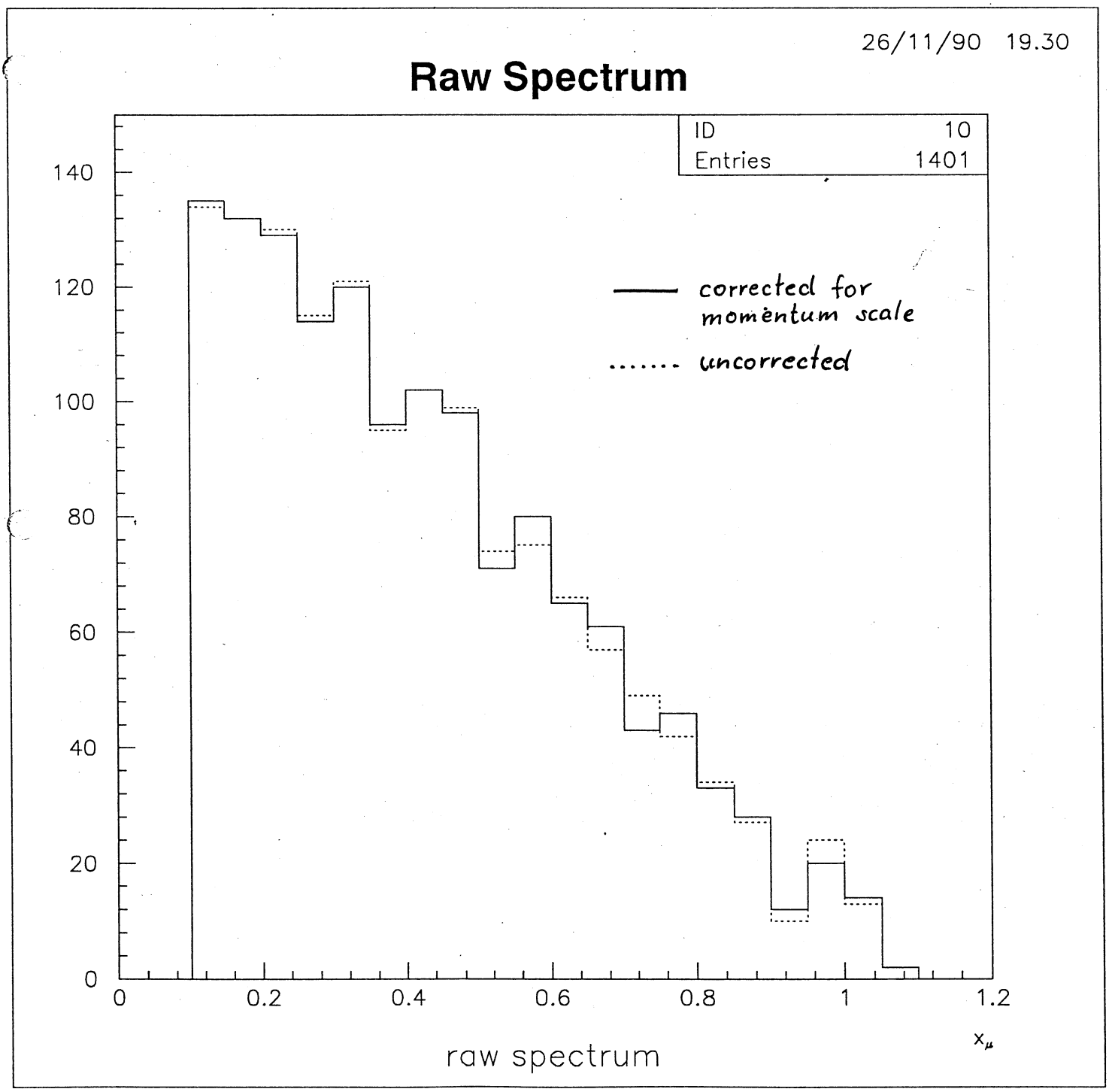
26/11/90 19.30
Raw Spectrum
ID 10
Entries 1401
corrected for momentum scale
uncorrected
140
120
100
80
60
40
20
0
0
0.2
0.4
0.6
0.8
1
1.2
x_μ
raw spectrum

Fig. 22

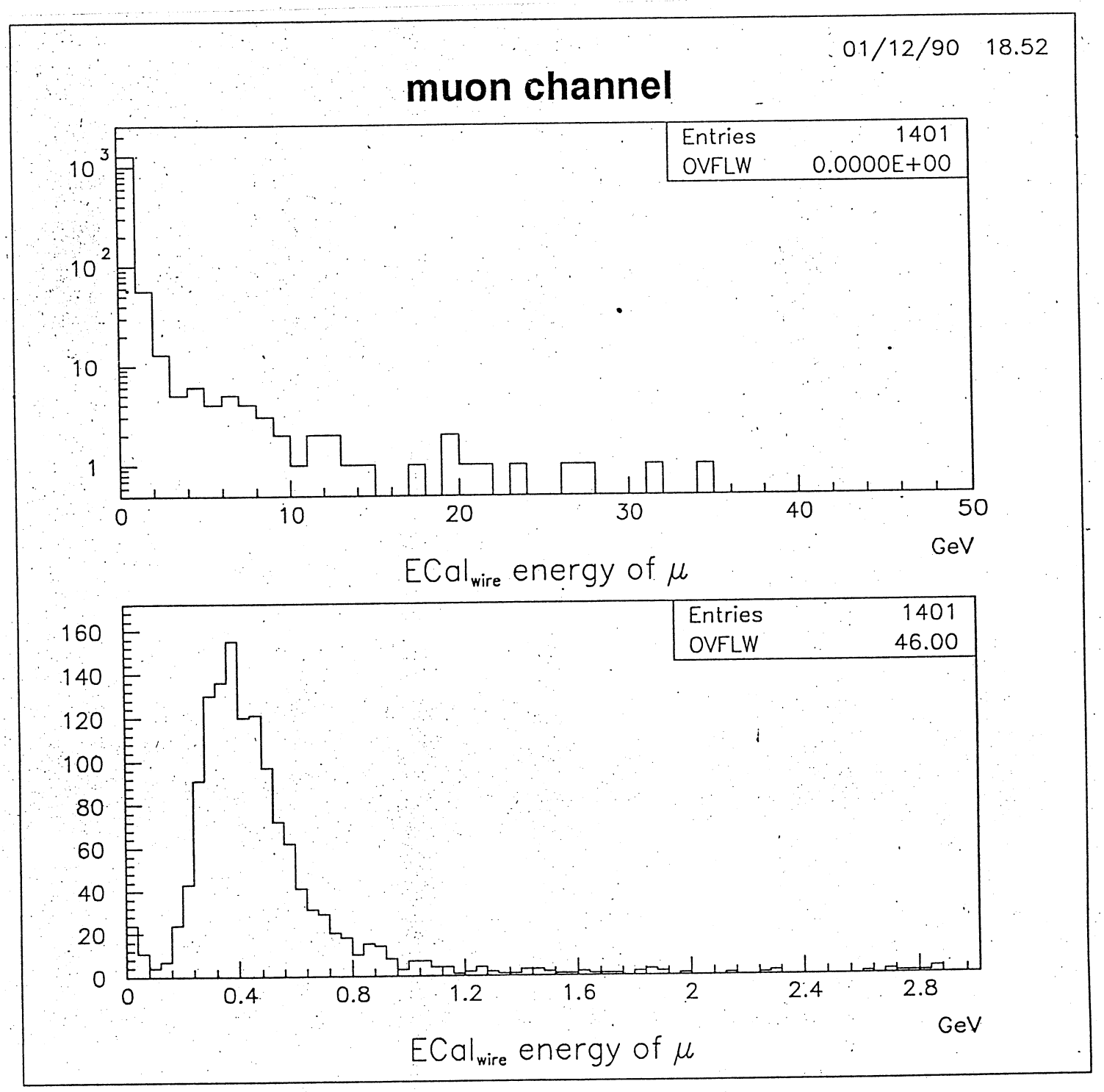
01/12/90 18.52
muon channel
Entries 1401
OVFLW 0.0000E+00
10 3
10 2
10
1
0
10
20
30
40
50
GeV
ECal wire energy of μ
Entries 1401
OVFLW 46.00
160
140
120
100
80
60
40
20
0
0
0.4
0.8
1.2
1.6
2
2.4
2.8
GeV
ECal wire energy of μ

Fig. 23

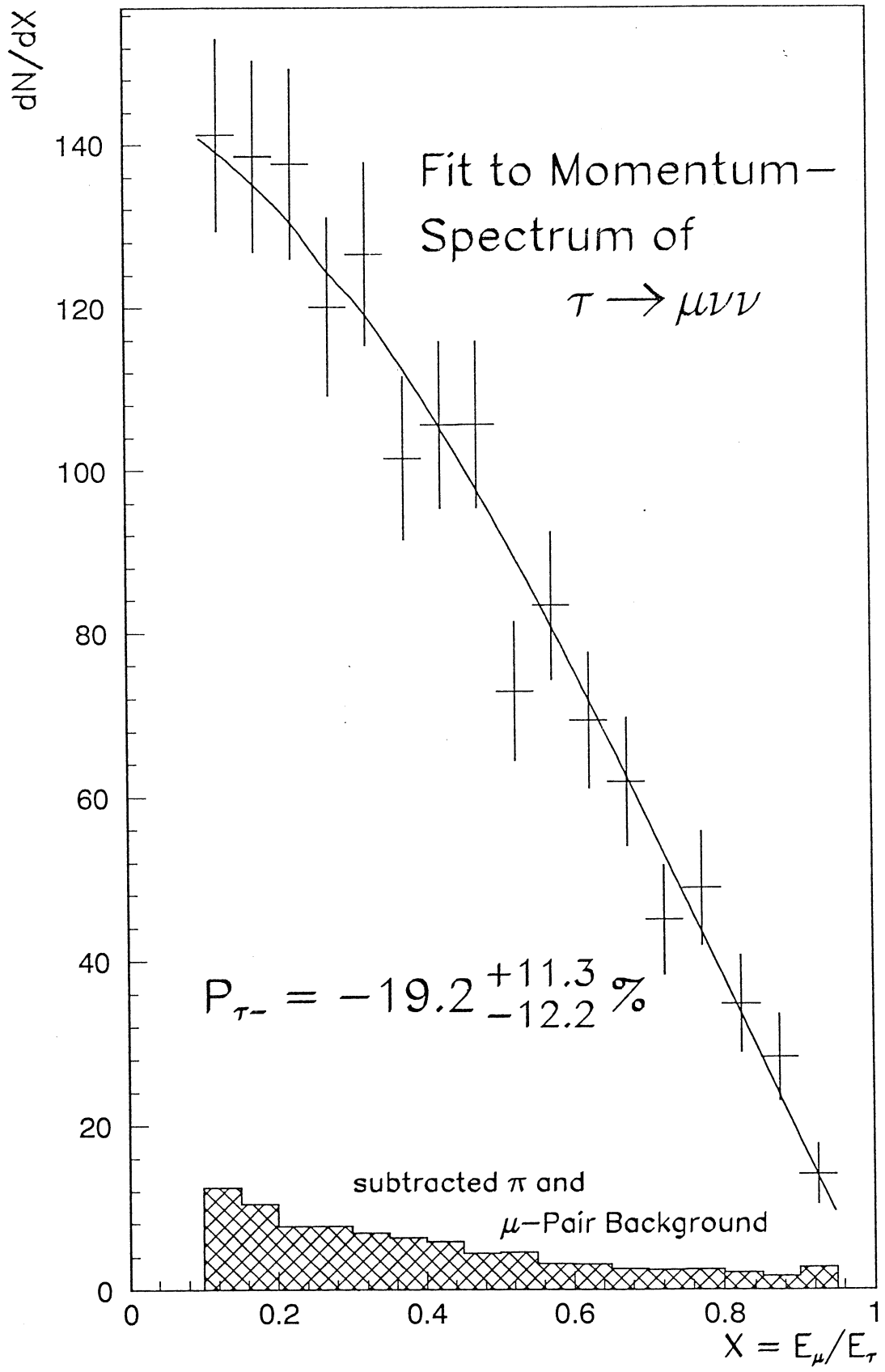
dN/dX
140
120
100
80
60
40
20
0
0
0.2
0.4
0.6
0.8
1
X = E_μ/E_τ
Fit to Momentum–
Spectrum of
$\tau \rightarrow \mu\nu\nu$
$P_{\tau^-} = -19.2\,^{+11.3}_{-12.2}\,\%$
subtracted π and
μ–Pair Background